ADVANCED MATERIALS
www.advmat.de

Carbon Dioxide Capture by Emerging Innovative Polymers: Status and Perspectives

*Made Ganesh Darmayanti, Kellie L. Tuck, and San H. Thang**

A significant amount of research has been conducted in carbon dioxide (CO_2) capture, particularly over the past decade, and continues to evolve. This review presents the most recent advancements in synthetic methodologies and CO_2 capture capabilities of diverse polymer-based substances, which includes the amine-based polymers, porous organic polymers, and polymeric membranes, covering publications in the last 5 years (2019–2024). It aims to assist researchers with new insights and approaches to develop innovative polymer-based materials with improved capturing CO_2 capacity, efficiency, sustainability, and cost-effective, thereby addressing the current obstacles in carbon capture and storage to sooner meeting the net-zero CO_2 emission target.

1. Introduction

1.1. Significance of CO_2 Capture

Carbon dioxide (CO_2) gas has long been considered as one of the greenhouse gases that contributes to climate change and the rise in the global average temperature.[1] In 2021, the world's CO_2 emission reached up to 33 884 million tons, which was driven by economic growth.[2] The main sources of CO_2 gas emissions, by sectors, are from energy (electricity, heat, and transport) (73.2%), direct industrial processes (5.2%), waste (3.2%), and finally agriculture, forestry, and land use combined (18.4%).[3] According to the Intergovernmental Panel on Climate Change (IPCC), CO_2 gas emission must be reduced to zero by 2050 to avoid the worst effects of climate change.[4] In order to achieve this net-zero CO_2 emission strategy by 2050, supreme efforts are needed rapidly and urgently. Efficiency improvements, renewable energy, and nuclear power, are all alternative options. However, these approaches are considered very costly to scaling-up, and lacking public support. Moreover there are activities such as aviation and iron smelting, that are impossible to run without releasing CO_2.[5]

Over the past few decades, there has been a global effort to develop new techniques for point source carbon capture, with the goal of preventing the release of CO_2 emissions into the atmosphere. Particularly, the technology that has garnered significant attention, and is expected to be a key factor in the evolution toward low-carbon energy use, is carbon capture, utilization, and storage (CCUS). CCUS was (2019) also acknowledged as one of the most cost-effective solutions in achieving large-scale emission reductions in the International Energy Agency (IEA) Clean Technology Scenario, which outlines a pathway to the sustainable industrial transformation, consistent to the Paris Agreement climate ambition.[6] Within the scope of the CCUS value chain, the CO_2 capture stage alone accounts for ≈70%–90% of the total operating CCUS costs. Therefore, CO_2 capture is a pivotal research focus for maturing the overall technologies and playing a significant role in reaching net-zero emissions.[7]

1.2. General Methods for CO_2 Capture

In general, CO_2 capture can be classified into three major processes: precombustion capture, oxyfuel combustion capture, and postcombustion capture as illustrated in **Figure 1a**.[8,9] The selection of the appropriate CO_2 capture strategy depends on various factors, such as the temperature and pressure of the CO_2 point sources, the partial concentration and partial pressure of CO_2, levels of impurities and pollutants, efficiency of the capture process, costs involved, and the environmental impact of the method.[10–12] The primary uses of these CO_2 capture strategies are expected to be at facilities where significant point amounts of CO_2 are produced, such as fossil fuel power stations, fuel processing facilities, and various industrial sites, especially those involved in iron, steel, cement, and bulk chemicals production.[11]

Postcombustion capture refers to CO_2 capture from flue gases generated by fossil fuel and biomass in air combustion. In this method, instead of releasing the flue gas containing nearly 5%–15% CO_2 directly into the atmosphere, it is directed through systems which separates the majority of CO_2. This CO_2 is then

M. G. Darmayanti, K. L. Tuck, S. H. Thang
School of Chemistry
Monash University
Clayton Campus
Victoria 3800, Australia
E-mail: san.thang@monash.edu
M. G. Darmayanti
Faculty of Mathematics and Natural Sciences
University of Mataram
Jalan Majapahit 62 Mataram, Nusa Tenggara Barat 83125, Indonesia

The ORCID identification number(s) for the author(s) of this article can be found under https://doi.org/10.1002/adma.202403324

DOI: 10.1002/adma.202403324

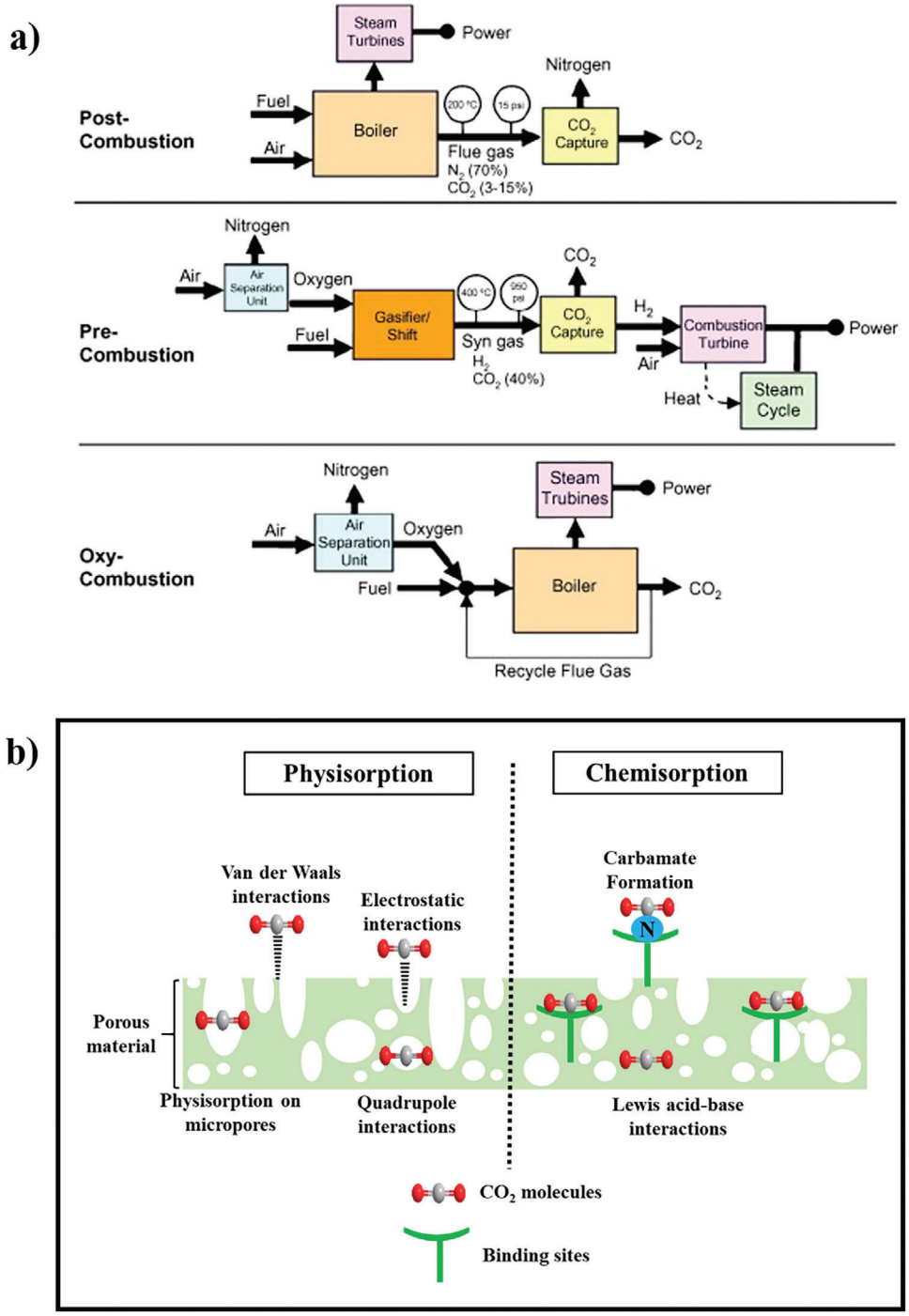

Figure 1. a) General methods of CO_2 capture technologies, including post-combustion, precombustion, and oxyfuel combustion capture. Reproduced with permission.[14] Copyright 2007, Elsevier. b) Mechanisms of CO_2 capture by porous material adsorbents.

transferred to a storage reservoir, and the residual flue gas is emitted into the atmosphere.[11,12] Postcombustion capture includes a broad range of CO_2 separation methods, such as absorption, adsorption, membrane, and cryogenics, which can be used without interrupting existing processes. This strategy can be integrated into existing plants through retrofitting and thus sustainably implemented in full-scale commercial facilities. Therefore, postcombustion capture is the commonly utilized strategy in CCUS projects.[9,13]

Precombustion capture refers to converting fuel into CO_2 and hydrogen. The process involves reaction of fuel with oxygen or air and/or steam to produce a "synthesis gas (syngas)" composed primarily of carbon monoxide (CO) and hydrogen. CO then undergoes a reaction with steam in a catalytic reactor, known as a

shift converter to give CO_2 and additional hydrogen. The CO_2 gas, concentration between 15% and 50%, is then separated through either physical or chemical absorption, leading to production of a hydrogen-rich fuel suitable for various applications, such as boilers, furnaces, gas turbines, engines, and fuel cells.[11,12] However, this process still faces challenges, including limitations of commercial availability.[14]

Instead of air, oxyfuel combustion capture utilizes pure oxygen during the combustion process to produce nearly pure CO_2. The process of burning fuel in pure oxygen results in an excessively high flame temperature, that can be moderated by recycling CO_2-rich flue gas back to the combustor. Typically, oxygen is generated through low temperature (cryogenic) air separation. Innovative methods for delivering oxygen to the fuel, such as membrane technologies and chemical looping cycles, are currently under development.[11] However, while the CO_2 concentration generated from the oxyfuel process is as high as 90%, this process is not as favorable as other capture technologies due to the high expenses associated with air separation required to obtain pure oxygen.[15]

An alternative method for addressing climate change is directly capturing CO_2 from the atmosphere through direct air capture (DAC).[16] Given the extremely low concentration of CO_2 in the atmosphere, chemical sorbents with strong binding capabilities are necessary. The main DAC systems use high temperature aqueous solutions and low temperature solid sorbent which are available from several industrial DAC developers, such as Carbon Engineering in Canada, Climeworks in Switzerland, and Global Thermostat in USA.[17] Although DAC is a relatively new technology, in its early commercial stages, it appears to be more energy extensive and costly. However, combined with conventional technologies, it offers a long-term solution that could assist humanity in managing and mitigating climate change.[18]

1.3. Materials for CO_2 Capture

In order to obtain further understandings of CO_2 capture by adsorbents, it is essential to discuss the mechanisms involved. Figure 1b illustrates the possible mechanism of CO_2 capture by porous adsorbents, encompassing physisorption, and chemisorption. Physical adsorption, or physisorption, is characterized as a reversible process, in which CO_2 are bound to adsorbents predominantly governed by Van der Waals forces,[19] or a combination with electrostatic interactions, quadrupole interactions, and the process of pore-filling. Physisorption is significantly influenced by the adsorption temperature and pressure, as well as the textural characteristics of the adsorbents, such as pore size and surface area. The pores are categorized into macropores (>50 nm), mesopores (2–50 nm), and micropores (<2 nm).[20] At low adsorption pressures, the pore volume-filling mechanism is the primary driven-force of the adsorption process, with micropores playing a significant role in CO_2 adsorption. In contrast, chemical adsorption or chemisorption involves the formation of new chemical bonds between CO_2 and the adsorbents. It generally involves Lewis acid-base interactions, facilitating the formation of covalent coordination bonds between CO_2 and the adsorbent surface, and are often enhanced by amine groups or nitrogen-containing materials leading to carbamate ion formations.[21] The effectiveness of chemisorption is influenced by the nucleophilic characteristics of the adsorbents' functional groups, while the reversibility of the capture is dependent on the binding strength, measured by the isosteric heat of adsorption (Q_{st}), where stronger bonds require more energy for adsorbent regeneration.[22]

The criteria for selecting materials for CO_2 capture depends on the specific application. Commercial postcombustion CO_2 capture systems, for example, relies on the original patent[23] principle in which a Brønsted base that is dispersed in an aqueous solution interacts with acidic gases in the flue gas stream. This method entails absorbing CO_2 gas into a low-volatility amine solution at room temperature. The amine is then regenerated by stripping it with water vapor at temperatures between 100 and 120 °C.[24,25] Aqueous solutions of monoethanolamine (MEA) and piperazine are standard amine solutions for this technology. This method of aqueous amine capture, however, present several major limitations, including corrosive issues, costly system designs necessary for durability and regeneration, and material lifespan or stability issues that necessitate the use of additives, thus making them cost-ineffective for its implementation on existing power plants.[24,26] Therefore, alternative materials have been extensively explored over the last decade to address the challenges associated with CO_2 capture.

Generally, the chosen materials should possess high capacity to efficiently adsorb CO_2, high selectivity toward CO_2, high chemical and thermal stability, good kinetics of adsorption and desorption, pore characteristics comparable to CO_2 molecules of being adsorbed, good regeneration capacity, and cost-effective.[7] Potential materials to fulfil these criteria for CO_2 capture include porous carbons,[27] zeolites,[28] metal–organic frameworks (MOFs),[29] and ionic liquid (IL).[30] Porous carbons and zeolites are promising candidates for both post- and precombustion CO_2 capture, due to their large surface area with good chemical and thermal stability.[31] Both of these materials are more energy efficient compared to aqueous amine solutions, by the absence of new chemical bonds of sorbate and sorbent, which leads to less regeneration energy demand. However, despite their impressive capacity for absorbing CO_2, porous carbons are limited by their relatively low CO_2/N_2 selectivity, while zeolites suffer the same as a consequence of their hydrophilic properties and affinity for moisture.[32] Meanwhile, MOFs, which are composed of metal nodes and organic linkers connected by coordination bonds, have open metal sites that can amplify the effective charge on the metal, thereby strengthening the interaction with CO_2 molecules resulting in enhanced CO_2 adsorption. They also exhibit well-defined structure, permanent porosity, and impressive tunability. However, being comprised of soft Lewis acids and hard Lewis bases, MOFs often experience limitations in physicochemical stability. Moreover, their structural framework hydrophilicity allows competitive adsorption with water, which strongly impacts their CO_2 capture capability.[31,32] Currently, ILs are gaining prominence as chemical absorbents in post- and precombustion CO_2 capture, attributed to their substantial solubility, a variety of liquid forms, tunability, and thermal stability. ILs are substances composed of entirely ions and possess a melting point below 100 °C. The first IL was ethylammonium nitrate, reported by Paul Walden in 1914.[33] ILs have the capability to capture CO_2 through either physical or chemical absorption methods.[32,34] One

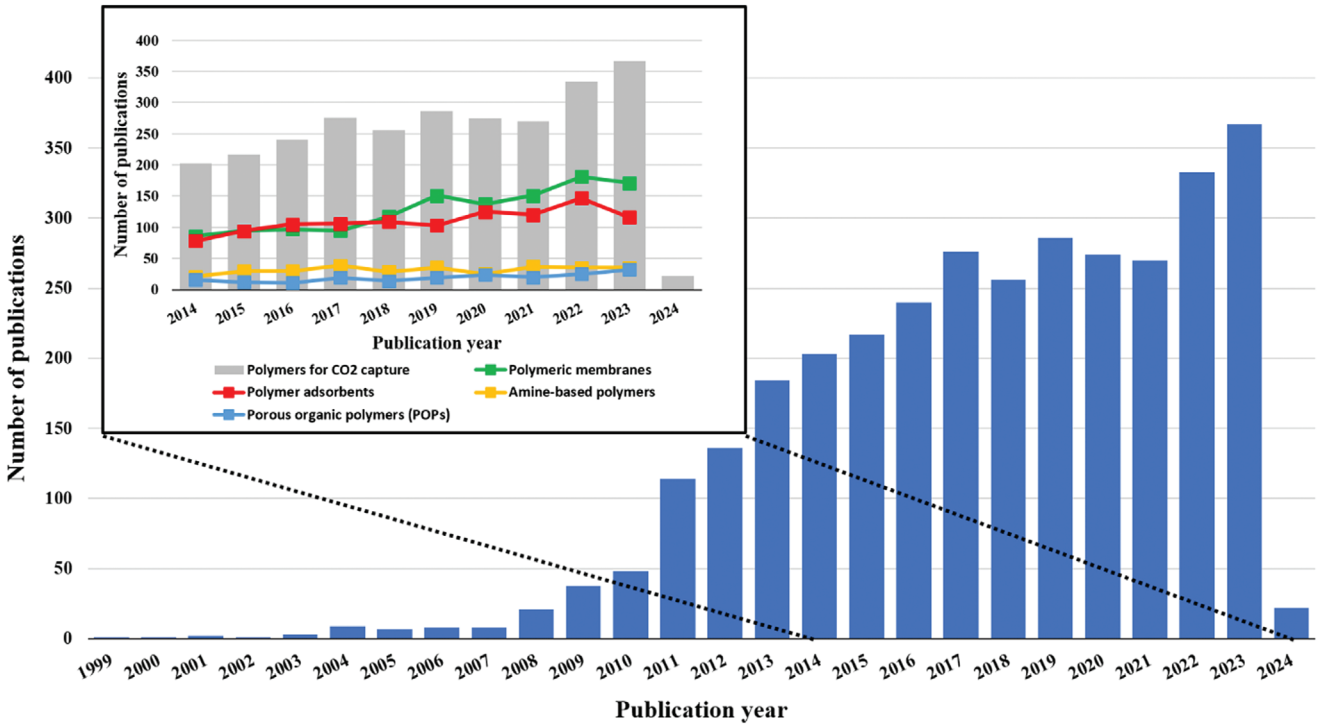

Figure 2. Number of publications on polymer-based materials for CO_2 capture for the years 1999–2024. Inset: The number of publications on the specific topic-related of the polymer-based materials for CO_2 capture, including polymeric membranes, polymer adsorbents, amine-based polymers, and porous organic polymers (POPs), over the last 10 years (2014–2024). Source: SciFinder^n (January 17, 2024). Command string keywords: polymer* and "CO_2 capture" with filter "publication year 2014 to 2024," (polymer and membrane and "CO_2 capture") or (polymer and membrane and "CO_2 separation:), (polymer and "CO_2 adsorption") or (polymer and adsorbent and "CO_2 capture"), (polymer and amine and "CO_2 capture") or (polymer and amine and "CO_2 adsorption"), ("porous organic polymers" and "CO_2 capture") or ("porous organic polymers" and "CO_2 adsorption").

limitation in using ILs for CO_2 capture is their elevated viscosity. Their high viscosity leads to slower absorption rate of CO_2 and typically higher pumping costs which hinders their suitability for industrial CO_2 capture applications.[35] As all of these emerging materials shows merits and demerits, research into improvements and enhancements of their properties is ongoing in the hope that optimum CO_2 adsorption capacity will be achieved.

Polymer-based materials have also been utilized for CO_2 capture. Their implementation in all CO_2 capture applications, from precombustion capture, oxyfuel processes to postcombustion capture, as well as for DAC, have been intensively studied and developed. They have been shown to have good to excellent CO_2 capture performances. Several key reasons of utilizing polymer-based materials for CO_2 capture are as follows:

i. *High selectivity toward CO_2*. Polymers can be engineered to have high affinity for CO_2, for example as membranes, resulting in good selectivity from gas mixtures.
ii. *Tunability*. The chemical and physical properties of polymers can be tailored to specific needs, including adjusting their porosity, surface area, and functional groups to optimize CO_2 capture.
iii. *Regenerability and durability*. Many polymers can be regenerated after CO_2 capture, meaning that they are able to release the captured CO_2 and be reused multiple times, which is essential for economic viability. Polymers can be modified to exhibit good chemical and thermal stability, allowing them to be durable over long periods of implementation.
iv. *Energy effective for regeneration*. The energy required to regenerate polymer-based materials and release the captured CO_2 is often lower compared to other materials like zeolites or amine solutions.
v. *Scalability and integration process*. Polymer materials can be produced on a large scale and can be easily integrated into existing industrial processes, which is important for the widespread adoption of CO_2 capture technologies.
vi. *Reduced environmental impact*. Polymers are potentially less toxic than conventional materials and engineered to be more energy-efficient, offering a reduced environmental impact.
vii. *Cost-effectiveness*. The synthesis, modification, and processing of polymer-based materials for CO_2 capture can be cost-effective, through simple polymerization reactions or the utilization of biopolymers. This is crucial for the commercial viability of CO_2 capture technologies.

The number of publications on polymer-based materials for CO_2 capture has increased significantly over the years, as displayed in **Figure 2**. Specific topics of these polymer materials from 2014 to the beginning of 2024, includes polymeric-based materials as membranes in the CO_2 capture, polymers as adsorbents in CO_2 adsorption, amine-based polymers for CO_2 capture, and porous organic polymers (POPs). While research in polymer-based materials are growing rapidly, recent reviews on

CO_2 capture tends to cover a broad range of materials. In contrast, this work aims to concentrate specifically on polymer-based materials, exploring their potential as effective candidates for CO_2 capture. This review provides a summary of the most recent polymer-based materials and their CO_2 performances in a wide range of CO_2 capture applications over the last 5 years. We also include up-to-date findings of advanced polymer-based materials that have been developed for CO_2 capture. Furthermore, our work includes alternative synthesis pathways of polymeric materials for CO_2 capture as new insights and approaches for researchers to creatively design new advanced polymer-based materials with improved CO_2 capacity, efficiency, sustainability, and cost-effective. The outlook of challenges and future trends of polymer-based materials is also proposed to address the current obstacles in CCUS technologies. The latest developments of polymer-based materials for CO_2 capture are outlined in Section 2 with alternative strategies for their syntheses described in Section 3.

2. Latest Developments of Polymer-Based Materials for CO_2 Capture

2.1. Amine-Based Polymers

Commonly, the CO_2 capture process involves two main phases: i) the selective reaction that allows separation of CO_2 from a gas mixture, and ii) the reversal of this reaction to regenerate the CO_2 capture material.[36] Efficient CO_2 capture hinges on the reversibility of this process. To reiterate, a weak interaction with CO_2 is inadequate for the capture process, due to this resulting in low selectivity and capacity. Conversely a strong interaction with CO_2 is also nonideal as typically results in an irreversible process under normal conditions. Therefore, a key criterion for the development of such materials is the "just-right principle," where materials interact moderately with CO_2 to attain effective CO_2 capture.[37]

Amines are commonly utilized as reagents in CO_2-selective materials owing to the moderate interaction between amine and CO_2. In this process, CO_2, acting as an electrophile, forms a zwitterion after reaction reacting with either a primary or secondary amine.[38] The zwitterion rapidly undergoes intramolecular proton transfer to form carbamic acid, which involves the transfer of an acidic proton. Subsequently, another amine deprotonates the carbamic acid, leading to the formation of stable carbamate and ammonium ion. The total mechanism requires 2 moles of primary or secondary amine for 1 mole of CO_2 as displayed in **Figure 3a**.

The stability of the carbamate species is influenced by the steric hindrance in the C—N bond. When the amine is sterically hindered, its bulky substituents limit the rotation of the C—N bond.[40] As a result, the carbamate becomes more likely to undergo hydrolysis, leading to the formation of bicarbonate and the regeneration of the amine.[41] In this reaction, only 1 mole of sterically hindered amine is required for 1 mole of CO_2. Therefore, sterically hindered amines demonstrate a higher CO_2 loading capacity compared to unhindered amines, although their reaction kinetics are slower.

Moreover, a tertiary amine cannot take part in a nucleophilic reaction with CO_2 because of the absence of labile proton. Instead, it acts as a Brønsted base which reacts with the carbonic acid formed by the reaction of CO_2 and water (Figure 3b).[42] The reaction requires 1 mole of tertiary amine for 1 mole of CO_2. This implies that tertiary amines present an advantageous reaction stoichiometry compared to primary and secondary amines, even though the reaction kinetics are slightly slower. Additionally, breaking the strong C—N bond in the carbamate formed from the reaction of primary and secondary amines with CO_2 is challenging. While for tertiary amines, it generates bicarbonate in which the C—N bond is easier to break, leading to a lower energy requirement for regeneration.[43]

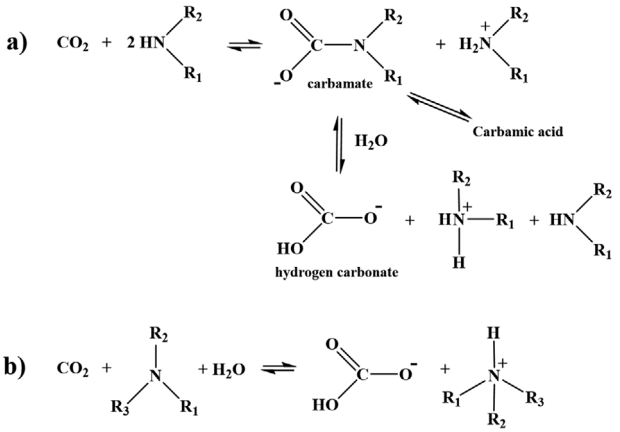

Figure 3. General scheme of CO_2 reaction with a) primary (R_1 = aliphatic; R_2 = H) and secondary amine (R_1, R_2 = aliphatic) and b) tertiary amine (R_1, R_2, R_3 = aliphatic). Adapted with permission.[39] Copyright 2010, John Wiley and Sons.

Due to the rich amine-CO_2 interaction, different types of polyamines have been extensively explored in the field of CO_2 capture. Herein, we have summarized the mostly studied polyamines and their recent developments in the last 5 years, including polyethyleneimine (PEI), polyvinylamine (PVAm), and polyacrylonitrile (PAN), which were specifically tailored and modified, leveraging the unique properties of amine groups for efficient CO_2 adsorption.

2.1.1. Polyethyleneimine (PEI)

PEI is a polymer with each repeating unit consisting of an amine group and two aliphatic CH_2—CH_2 spacers. It is available as either linear, branched, or dendrimer PEIs.[44] The significance of PEI in CO_2 capture was first noted in the seminal report by Satyapal et al. in 2001, highlighting its usage for CO_2 removal in space life support applications.[45] Since then, PEI has attracted widespread interest and has become the most studied of aliphatic polymeric amines for CO_2 sorption, in the context of large-scale industrial use, from major point sources and also directly from the ambient air. This is attributed to its high number of amine groups, ease of synthesis, low cost,[44] low volatile hazards, high selectivity of CO_2,[46] regenerability, and versatility. Mostly, PEIs are loaded to support materials as solid adsorbents in the CO_2 adsorption process. The PEI-based solid sorbents primarily consist of a silica support that is impregnated with PEI. This composition is used in a circulating fluidized bed or a bubbling fluidized bed

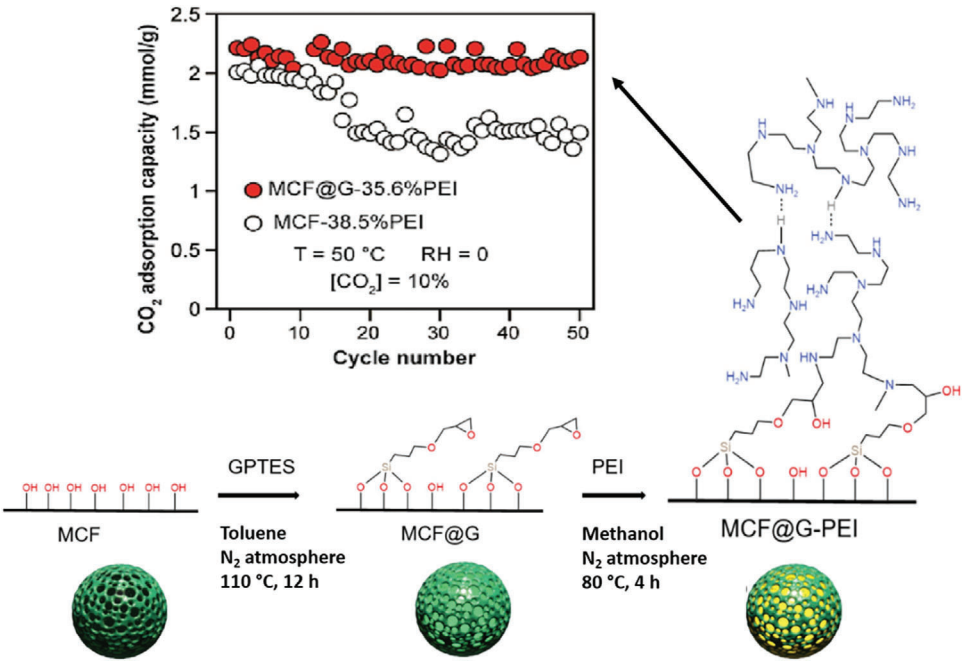

Figure 4. Synthetic route of PEI grafting onto the pores of a mesocellular silica foam (MCF) to obtain MCF@G-PEI and its CO_2 adsorption capacity after 50 adsorption–desorption cycles. Reproduced with permission.[51] Copyright 2023, Elsevier.

reactor for CO_2 capture.[47] Besides impregnation, other typical modifications include postsynthesis grafting and copolymerization which are suitable for membrane in gas separation.[44] Insights of PEI-based material modification, special features, and their specific application in CO_2 capture in the last 5 years are listed in **Table 1**. Key significant findings are discussed further below.

Impregnation of PEI on nanoporous hosts has been most thoroughly explored in the context of CO_2 adsorption.[48] The PEIs are physically loaded into accessible pores and on the surface of a porous support with no chemical bond forms between PEI and the support.[7] The use of solvent, such as water or organic solvents like methanol or ethanol, facilitates impregnation of the amine with the support. Choi et al. reported wet impregnation of PEI on MOFs immobilized polyacrylonitrile (PAN) fiber mats.[49] It was concluded that by the addition of PEI, the CO_2 adsorption capacity significantly increased by 45% compared to the original PAN/MOF, resulting in a high increase in CO_2/N_2 sorption selectivity from 6 to 54. Jia and co-workers, synthesized a mesoporous MCM-41 material derived from spent fluid catalytic cracking catalyst functionalized by PEI through impregnation which can be applied for dilute source CO_2 capture processes.[50] The obtained material demonstrated an acceptable equilibrium CO_2 capacity of 2.7 mml g^{-1} in 10% CO_2/N_2 simulated flue gas at 65 °C, showing excellent cyclic stability during 50 temperature swing adsorption (TSA) cycles in simulated dry flue gases.

While impregnation entails physical interaction between the PEI and the porous support, the grafting method involves a covalent bonding process, in order to attach PEI to the functional groups of the support material. Shi et al. reported the co-grafting of PEI onto the inner pores of a mesocellular silica foam (MCF) using (3-glycidyloxypropyl)triethoxysilane (GPTES) as a bridging medium.[51] This solid sorbent, denoted as MCF@G-PEI, showed great potential for CO_2 capture from flue gas streams as it exhibited a maximum CO_2 adsorption capacity of 2.78 mmol g^{-1} at 50 °C. As shown in **Figure 4** the MCF@G-PEI with 35.6% PEI-grafted loading maintained an excellent long-term stability over 50 consecutive cycles, compared to the MCF-38.5%PEI prepared by direct physical impregnation without GPTES, in which its CO_2 adsorption capacity significantly decreased after 15 cycles. This result confirms the advantage of covalently-bonded PEI via cografting in enhancing the adsorption of CO_2. Li and co-workers, prepared a microporous organic adsorbent showing satisfactory potential by grafting PEI onto a core–shell structure of poly(acrylamide) as the skeleton, poly(glycidyl methacrylate) as the shell, and F-127 and pluronic block copolymer as the surfactant.[52] This material displayed high adsorption capacity and fast adsorption kinetics, with great thermal stability and selectivity. With 50 wt% PEI loading to the core–shell, the CO_2 capture capacity reached 3.11 mmol g^{-1} at 40 °C, and desorption completed at 80 °C. In another report, Justin et al. applied a two-step postsynthetic modification (PSM) strategy to covalently graft PEI to the amino-ligand inside of a Cr-MOF.[53] The use of bromoacetyl bromide as the bridging medium resulted in the best adsorbent material in this study, denoted as PEI-Ac-NH-Cr-BDC-Washed, exhibiting 1.55 mmol g^{-1} CO_2 uptake at 313 K and 0.15 bar and an ideal-adsorption-solution-theory (IAST) CO_2/N_2 selectivity of 437.

In terms of modifying PEI-based CO_2 adsorbents, it is also important to consider the structure of the support material. Li et al. investigated the influence of different silica nanostructure supports for PEI-functionalized adsorbents, in the form of silica nanospheres (SNPs), silica nanosheets (SNHs), and silica nanotubes (SNTs).[54] It was shown that the morphology of support

Table 1. PEI-based materials, special features, and their specific application in CO_2 capture.

PEI-based materials	PEI type	CO_2 performance	Special features	Application	Refs.
PEI-impregnated-MOFs immobilized PAN fiber mats	Branched PEI; $M_w = 600$; density = 1.05 g mL^{-1}	CO_2 adsorption capacity increased 45% compared to original PAN/MOF and CO_2/N_2 selectivity of 54	• Increased surface area • Improved CO_2 adsorption capacity and CO_2/N_2 selectivity at very low pressures	CO_2 adsorption (solid sorbent)	[49]
PEI-impregnated-spent fluid catalytic cracking catalyst derived MCM-41	Branched PEI; $M_n = 600$	Equilibrium CO_2 capacity of 2.7 mmol g^{-1} at 65 °C	Adsorption capacity maintained constant in 50 TSA cycles	Dilute source CO_2 capture processes	[50]
PEI-grafted-mesocellular silica foam (MCF@G-PEI)	Branched PEI; average M_n = 10 000	CO_2 adsorption capacity of 2.78 mmol g^{-1} at 50 °C and 50% relative humidity (RH)	Superior reusability in 50 consecutive cycles	CO_2 adsorption (solid sorbent)	[51]
PEI-grafted on microporous core–shell copolymer beads	[a]	CO_2 capture capacity reached 3.11 mmol g^{-1} at 40 °C	• High adsorption capacity and fast adsorption kinetics • Great thermal stability and selectivity	CO_2 adsorption (solid sorbent)	[52]
PEI-grafted to a Cr-MOF (PEI-Ac-NH-Cr-BDC-Washed)	[a] $M_w = 600$	1.55 mmol g^{-1} CO_2 uptake at 313 K and 0.15 bar and an IAST CO_2/N_2 selectivity of 437	High CO_2 capacity over 200 TSA cycles in humid flue gas	CO_2 adsorption (solid sorbent)	[53]
PEI-functionalized nanostructured SiO_2	[a] $M_w = 600$	CO_2 adsorption capacity of 3.68 mmol g^{-1}	Low adsorption heat and regeneration energy	CO_2 adsorption (solid sorbent)	[54]
Ceramic fiber honeycomb coated PEI-impregnated mesoporous cellular foam adsorbent (using hydrophobic polystyrene-*b*-polybutadiene-*b*-polystyrene (SBS) as binder)	Branched PEI; $M_w = 600$ g mol^{-1}	CO_2 uptake of 0.71 mmol g^{-1} composite (2.33 mmol g^{-1} adsorbent) in 400 ppm CO_2	• Stable throughout 100 cycles, mechanically robust under air blowing • Low energy consumption of 0.196 MJ mol^{-1} and high productivity of 5.60 mol kg^{-1} day^{-1} in steam-assisted temperature swing adsorption (S-TSA) processes by simulations	DAC scale-up deployments	[56]
Supported mixed diethanolamine (DEA)/PEI (1:1) on SBA-15 adsorbent	[a] Average $M_n = 600$ by GPC	Maximum CO_2 uptake of 1.62 mmol g^{-1} (46% higher than supported PEI with same amine loading)	• Fast desorption kinetics at temperatures as low as 70 °C • Maintaining high thermal and chemical stability over 50 DAC cycles • Outstanding adsorption performance even at cold temperature (−5 °C)	DAC	[57]
PEI-impregnated γ-Al_2O_3	Branched PEI; $M_w \approx 800$; $M_n \approx 600$	CO_2 uptake of 1 mmol g^{-1} at 25 °C	Maintained CO_2 capacity at both −20 and 25 °C of multiple TSA cycles under dry conditions	DAC	[58]
PEI-impregnated quasi-1D hierarchical zeolite nanotubes	Branched PEI; $M_w = 800$ g mol^{-1}	Identical CO_2 uptake of ≈2.2 mmol g^{-1} at two different CO_2 concentrations (400 ppm and 10% CO_2)	• Stable performance over multiple TSA cycles • CO_2 uptake increases up to 25% at intermediate RH	DAC under ambient conditions	[59]
PEI-crosslinked cellulose (PCC) aerogel sorbent	[a] $M_w = 600$	CO_2 adsorption capacity reached 2.31 mmol g^{-1} at 25 °C under pure dry CO_2 atmosphere	• Excellent CO_2 adsorption-desorption recyclability after 10 cycles • Flexible and porous • Retained high specific surface area 234.5 m^2 g^{-1} at 17.4 wt% N_2 content	CO_2 adsorption (solid sorbent)	[60]

(*Continued*)

Table 1. (Continued)

PEI-based materials	PEI type	CO_2 performance	Special features	Application	Refs.
PEI/Zirconium bifunctionalized molecular sieve of KIT-6	[a]	Maximum CO_2 adsorption capacity of 174.7 mg g^{-1} at 25 °C and 40 mL min^{-1} gas flow rate	Adsorption level remains stable even after 20 cycles	CO_2 adsorption (solid sorbent)	[61]
PEI-impregnated lignin mesoporous cellular carbon	Branched PEI; M_w = 600	CO_2 uptake of 2.90–3.13 mmol g^{-1} at 75–90 °C and 0.15 bar	• Well-developed 3D interconnected porous structure with large pore size and pore volume (up to 1.80 cm^3 g^{-1}) • Exhibit superior thermo-stability	Post-combustion solid sorbent	[62]
Polystyrene sulfonate (PSS) stabilized PEI membranes by spray-coating	Branched PEI; M_w = 600 Da	CO_2 permeance ranging from 820 to 1770 GPU and CO_2/N_2 selectivity varying from 395 to 460 under vacuum operation mode at 80 and 90 °C	• Defect free selective layer • Good long-term stability • Successfully scaled up to 200 cm^2 with good uniformity	CO_2 membrane separation	[63]
PEI functionalized F-Ce nanosheets via electrostatic self-assembly mixed matrix membranes (MMMs)	Branched PEI; M_w = 600	CO_2 adsorption capacity 1.32 mmol g^{-1}; CO_2 permeability of 641 Barrer and CO_2/N_2 selectivity of 70.1	• Stable pore channel 3.406 nm nanosheets with improved CO_2 transport • CO_2 permselectivity values exceeding the 2019 upper bound	CO_2 membrane separation, specifically for cryogenic gas separation applications	[64]
PEI incorporated high-valence metal-induced microporous polymer (HMMP-1) nanoparticles as fillers for MMMs	Linear PEI; M_n = 2500; $Đ$<1.2	CO_2 permeance of 1544 GPU and CO_2/N_2 selectivity of 252 at 0.2 MPa feed gas (15/85 vol% CO_2/N_2 system)	• High Brunauer–Emmett–Teller (BET) specific surface area of HMMP-1 (787.84 m^2 g^{-1}) with homogeneous 0.9 nm pores • Good interfacial compatibility of HMMP-1 onto the polymer matrix • Facile membrane fabrication process	CO_2 membrane separation	[65]
Polysulfone (PSf)/PEI blend modified with phenyl isocyanate as additive	Hyperbranched PEI	Focuses on dielectric analysis studies	Better affinity to trap CO_2, better mobility favoring CO_2 conduction, and better hydrophilic stability	Membrane contactors	[66]

[a] PEI type not stated.

plays a crucial role in CO_2 capture from flue gas, particularly the key parameters associated with ultralow emission, such as adsorption capacity, amine efficiency, thermodynamics, kinetics, cyclic stability, and temperature of optimal adsorption. SNHs enhanced the dispersion of the PEI active sites for successful mass transfer resistance reduction of CO_2 during the adsorption process. SNTs increased the diffusion resistance of CO_2 leading toward decreased adsorbent performance. While for SNPs, the PEI loading into the pores was effective and demonstrated higher adsorption capacity of 3.68 mmol g^{-1}, along with a lower desorption heat of 51.91 kJ mol^{-1} and low energy requirement of 1.775 GJ ton^{-1} for regeneration.

One of the drawbacks of PEI-based adsorbents is oxidative degradation. During a standard temperature swing process, the CO_2 saturated adsorbent is regenerated at temperatures ranging from 100 to 110 °C, and subsequently cooled to the required adsorption temperature. Typically, the regeneration phase is conducted using steam, while the cooling phase is performed in air. The probability of oxidative degradation is significantly elevated during this cooling phase, as both temperature and oxygen levels are at their peak. This phenomenon not only occurs on PEI supported structures, but also other amine-based materials in aqueous solution. Furthermore, it has been discovered that commercial polyamines, including PEI, contain trace amounts of Fe or Cu metal cations, positively correlated to the rapid oxidation of PEI.[55] However, this undesirable oxidation process can be mitigated by the addition of poly(vinyl alcohol) (PVA) and epoxide functionalization of amines, which has been investigated by Yan and Sayari.[46] The observed antioxidative effect was attributed to the hydrogen bonds between amine groups and the hydroxyl groups in these polymers, which shields the amine groups from being attacked by oxygen. It appears that PVA and 1,2-epoxybutane (EB) have the ability to trap radicals, temporarily holding but not eliminating the radical centers. While not completing eliminating the presence of radicals, they are a barrier against the oxidation of PEI. Additionally, the formation of hydrogen bond between these agents and PEI increases their effectiveness at slowing oxidative degradation.

2.1.2. PVAm (Polyvinylamine)

PVAm is a linear polyelectrolyte polymer which has the highest possible density of pendant primary and secondary amines.[67] In the area of CO_2 capture, PVAm are utilized mostly as a matrix for facilitated transport membranes (FTMs). The amino groups in PVAm acts as fixed site carriers (FSC), enabling the CO_2 molecules to hop along, providing reactive diffusion pathways for CO_2 transport and enhancing the overall CO_2 chemisorption of the membrane. PVAm FTMs were initially developed by Kim et al. in 2004 by applying a thin selective layer on a flat-sheet polysulfone (PSf) support.[68] After years of optimization, the PVAm membranes were then applied to a pre-pilot demonstration of a coal-fired power plant in Norway (2013), under real flue gas conditions, and demonstrated good CO_2 permeance and stability over a 6.5 months period. In 2017, these PVAm flat sheet membranes were upgraded to hollow fiber membranes on a pilot scale to show 60–83 mol% CO_2 purity for 6 months, even under rigorous conditions with SO_2 and NO_x impurities.[69]

Regrettably, a primary drawback of PVAm lies in its mechanical fragility, especially when exposed to high water content.[67,70] Under these conditions, the self-standing PVAm membranes are susceptible to swelling and breaking, thus it is a challenge to use their pure form for FTMs applications. Consequently, numerous approaches have been developed to enhance the mechanical robustness of PVAm in order to achieve more durable membranes. Strategies such as crosslinking the matrix, employing polymers of higher molecular weight (MW), and incorporating nanomaterials to create mixed matrix composite membranes (MMCMs) have been explored as potential solutions.

Crosslinking of the polymer matrix is one approach to form sturdy membranes with better CO_2 permeability. Materials such as MOFs are often selected to be crosslinked onto the matrix. MOFs possess stable physical structures with abundant pores that are likely to be compatible with various polymer matrix. Ge and co-workers, crosslinked PVAm with MOF-808 by using KH-560 as the cross-linker, developing MMCMs with good operational stability, remarkable CO_2 permeance of 2753 GPU and selectivity of 181, in a CO_2/N_2 separation system at 2 bar.[71] Recently, for the first time, Shin et al. performed a reverse approach by loading PVAm onto a typical MOF with high porosity, MIL-101, via the ship-in-a-bottle (SIB) synthesis technique.[72] It was found that introducing an appropriate amount of PVAm significantly enhanced the CO_2/N_2 selectivity and CO_2 adsorption capacity at low pressure, achieving values up to 11 times higher than the pristine MIL-101 adsorbents.

Commercial PVAms are often unavailable for high-performance membrane fabrication, due to their low molecular weight and excessive crystallinity. As an alternative, using polymers with higher molecular weights and varying architectures are potential options to increase the membranes' mechanical strength. Yuan et al. refined the PVAm synthesis process by adjusting the polymerization and acidic hydrolytic conditions.[73] They obtained PVAm with a MW of 154 kDa (11.37% crystallinity) which was then developed as defect-free composite membranes that exhibited high CO_2 permeance of 726 GPU and CO_2/N_2 selectivity of 55 at 0.5 MPa feed gas pressure, with high potential to scaled-up manufacture. An ultrahigh MW PVAm for membrane fabrication was prepared by Chen and co-workers via inverse emulsion polymerization (IEP) (**Figure 5a**).[74] By this method, they successfully obtained PVAm from *N*-vinylformamide (NVF), with a MW of 12.7 MDa which further strengthen the polymer matrix and allowed the loading of piperazine glycinate (PG), as a mobile carrier, up to 85 wt%. The developed PVAm/PG composite membranes exhibited a CO_2 permeance of 839 GPU and a CO_2/N_2 selectivity of 161 at the standard flue gas temperature of 57 °C. Later on, this group also developed a sterically hindered PVAm-CH_3 membrane incorporated with an amino acid salt (2-(1-piperazinyl)ethylamine sarcosinate) (PZEA-Sar), acting as a mobile carrier, which was coated on a nanoporous poly(ethersulfone) (PES) substrate.[75] The resulting thin film composite (TFC) demonstrated a superior CO_2 permeance of 1071 GPU and a CO_2/N_2 selectivity of 183 at 57 °C, under a feed gas pressure of 111.64 kPa. This value exceeded the newly revised 2019 upper bound for CO_2/N_2 performance and surpassed other polymer-based membranes in efficacy, as displayed in **Figure 5b**.

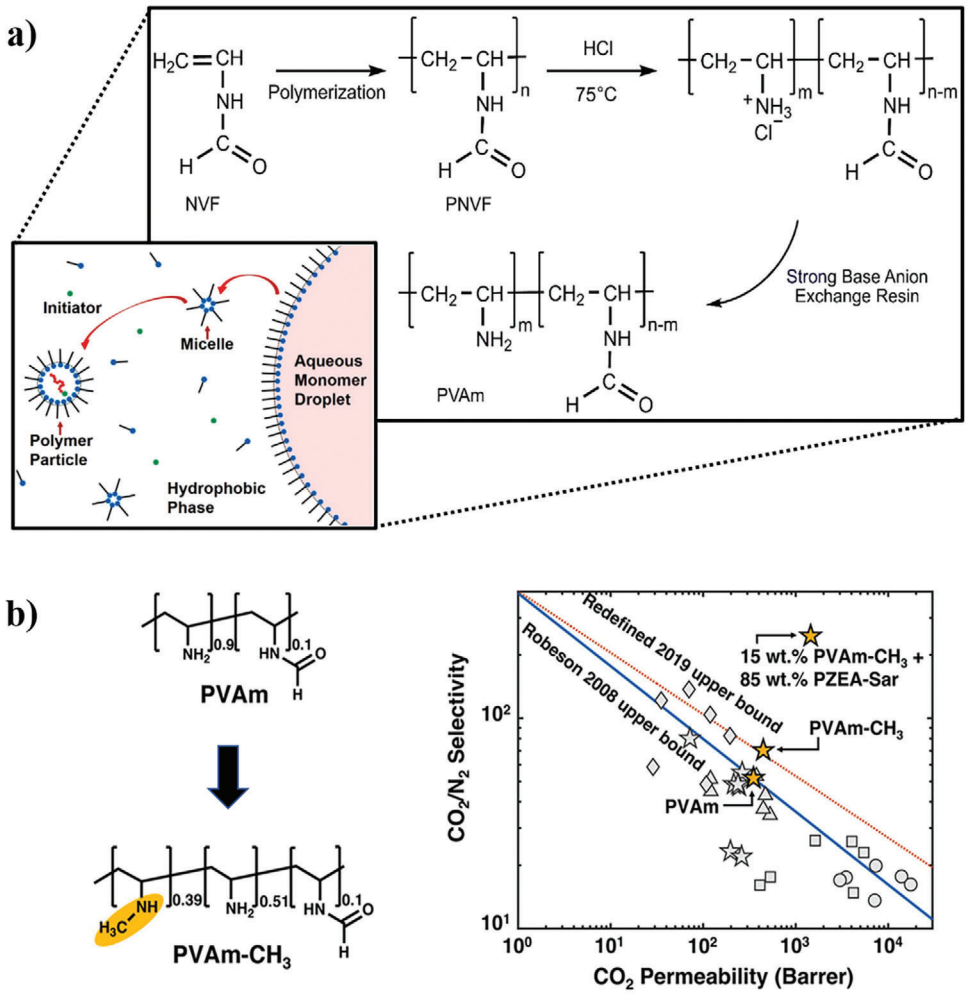

Figure 5. a) Schematic of PVAm synthesis from NVF via inverse emulsion polymerization (IEP). Reproduced with permission.[74] Copyright 2021, Elsevier. b) Structure of PVAm-CH_3 and comparison graph of PVAm-CH_3 and PVAm-CH_3 + PZEA-Sar with other materials for CO_2/N_2 separation, including amine-containing fixed-site carriers (FSC) (☆), poly(ethylene glycol) (PEO) based polymers (△), polymers of intrinsic microporosity (PIM) (○), thermally rearranged (TR) polymers (□), and mixed-matrix materials (MMM) (◇) in the Robeson 2008 upper bound and redefined 2019 upper bound. Reproduced with permission.[75] Copyright 2021, Elsevier.

Incorporating nanomaterials into a polymer matrix is a recent trend to achieve high performance CO_2 capture membranes. Nanoparticles such as graphene (G), carbon nanotubes, and MOFs provides high surface area, while the polymer matrix offers stability. Nanomaterials loading of graphene and graphene oxide (GO) nanofillers onto pure PVAm membranes has been reported by Casadei et al.[70] These sheet-like graphenic nanomaterials have been identified as excellent building blocks for the MMCMs, acting as a reinforcer additive to maintain the membranes' mechanical strength in conditions of high humidity, and also increasing its permeability and selectivity properties. The membranes permeation tests conducted at 35 °C and high relative humidity (95% RH), gave a maximum CO_2 permeability result of almost 70 Barrer for low grade PVAm + 3% GO and maximum CO_2/N_2 selectivity of about 81 for high grade PVAm + 3% GO. More recently, they also modified PVAm membranes by coupling it with the bio-based carboxymethylated-nanofibrillated cellulose (cNFC) and the addition of L-arginine as a mobile carrier.[76] The findings indicate that L-arginine addition reduces the membranes' water uptake due to the lower PVAm content, yet it strongly enhances the CO_2 transport. Experiments conducted at 35 °C and high RH resulted in a rise of CO_2 permeability which climbed up from 160 to about 340 Barrer when L-arginine loading was raised from 0 to 45 wt%. The achieved permeability was one of the highest recorded for PVAm/nanocellulose-based membranes, but the selectivity was lower than other reported FTMs.

Hybrid materials of PVAm and other polymers with CO_2 capture properties has also been studied recently. Aframehr et al., developed PVAm-polyimide (PI, Matrimid)-blend FTMs, incorporated with silica nanoparticles.[67] Their findings show that higher silica loadings gradually increased CH_4 and N_2 permeability. The developed FTMs has the potential to overcome the Robeson upper bound for both CO_2/CH_4 and CO_2/N_2 separation, while suggesting permeation tests in humidity conditions and with smaller particles to be further explored. Meanwhile,

Wang and co-workers, successfully developed MMCMs that exceeded the CO_2 permeance and CO_2/N_2 selectivity of the pristine PVAm membrane.[77] Their MMCMs were prepared by lamellar polyaniline-coated carbon nanotubes in GO layers mixed with PVAm, coated on an asymmetric PSf membrane. The MMCMs, referred as PVAm/PANI@CNTs-GO/PSf, demonstrated outstanding long-term stability, maintaining their performance under mixed-gas conditions for more than 300 h, achieving a CO_2 permeance of 264 GPU and CO_2/N_2 selectivity of 149.8. It is expected that this improved separation performance was attributed to the role of the facilitated transport carriers (i.e., amine groups) in the interlayer spacing and the molecular sieving effect provided by the interlayer spacing. Other PVAm-hybrid membrane materials, that are being developed recently, incorporate MOFs of zeolite imidazolate frameworks (ZIFs) as fillers due to its nanoporous structure, thus being able to differentiate and filter CO_2 from N_2. In this context, Zhang et al. developed porous PSf membrane-supported MMCMs via coating of ZIF-8-NENP-NH_2 and PVAm for efficient CO_2 and N_2 separation.[78] MMCMs loaded with 7 wt% ZIF-8@NENP-NH_2 demonstrated a notable CO_2 permeance of up to 301 GPU, coupled with a selectivity of 91, surpassing the 2019 upper bound. This represents a significant enhancement of 296.1% and 89.6%, respectively, compared to the pristine PVAm membrane. Moreover, after a period of 360 h using CO_2/N_2 mixed gas as the feed gas, this membrane maintained an average CO_2 permeance of 369 GPU and a CO_2/N_2 selectivity of 97.3. The findings suggest that the surface chemistry environment of the hierarchical pore in the shell and molecular sieving pore in the core, facilitated the CO_2 permeation. Likewise, Wang et al. fabricated MMCMs comprising partially amorphous ZIF-8-decorated metakaolin (ZIF-8-d-MK) dispersed in PVAm matrix, and then coated onto the PSf support membrane.[79] The findings showed that this modification of PVAm-based membranes, decorated with ZIF, successfully maintained its stability under long-term operation over 360 h. Moreover, the MMCMs also resulted in transcending the 2019 upper bound, with high CO_2 permeance up to 169 GPU and high CO_2/N_2 selectivity of 86.7.

2.1.3. Polyacrylonitrile (PAN)-Based Materials

PAN-based materials in the area of CO_2 capture are utilized mostly as nanofiber adsorbents. Unlike granular adsorbents, fiber-based adsorbents offer superior features, such as high exterior surface area, short transit distances, minimal pressure drops, and flexibility. Moreover, reducing the length of fibers from micro to nanosized can enhance the work capacity and efficiency of fibrous adsorbents.[80] PAN-based carbon nanofibers (CNFs) demonstrate excellent adsorption capacity and high selectivity, even under reduced pressure, due to its porous structure originating from their turbostatic structure which comprises numerous disordered stacks of graphitic layers. They are easily fabricated, generally carried out by electrospinning, stabilization, and carbonization processes. Electrospinning is a typical versatile and straightforward technique for fabricating nanofibers. Moreover, optimization of the CO_2 adsorption capacity in PAN-based CNFs can be developed by increasing the surface area, introducing nitrogen or amine functional groups by doping or grafting, and enhancing the presence of ultramicropores in which are significantly influenced by the carbonization temperature.[81]

Tetraethylenepentamine (TEPA) grafting onto PAN hollow fibers has been reported by Zhang and co-workers.[82] They employed the TEPA@PAN hollow fibers for DAC, due to their high CO_2 adsorption capacity that reached up to 3.66 mmol g^{-1} at low concentration of CO_2 (5000 ppm). Most recently, Zhang's group modified their previous work by hydrolyzing nitrile groups on the hollow PAN fiber surface and then chemically grafting TEPA on it.[83] Not only simplifying the preparation procedure and reducing the cost, this modification also enhanced the CO_2 adsorption capacity up to 5.07 mmol g^{-1} at low CO_2 concentration (5000 ppm), making them potential sorbents for CO_2 capture and separation from ambient air. Tourzani et al.[84] and Imanian et al.[85] reported γ-radiation induced grafting of glycidyl methacrylate (GMA) onto pristine PAN nanofibers and combined industrial PAN-polyurethane (PU) electrospun nanofibers, followed by amination with ethanolamine (EA). Similar findings were reported, that pristine PAN and PAN/PU nanofibers, in which both grafted with GMA-EA, achieved CO_2 adsorption capacity of 2.84 and 2.98 mmol g^{-1}, respectively, and maintained stable in several adsorption–desorption cycles at 80 °C. GMA is widely recognized as a valuable precursor monomer for graft copolymerization, as its epoxy group can be easily converted into other functional groups. Compared to conventional grafting techniques, radiation-induced graft copolymerization (RIGC) offers several advantages, which includes its process simplicity, the ability to have a finely adjust composition, capability to tailor properties and modify substrates of various morphologies (films, fibers, and textiles), also its lack of use of chemical initiators.[86] In the process of RIGC, the side chain is covalently bonded from a monomer to a polymer backbone to obtain the branched copolymer and the active radicals on the polymer matrix are generated through exposure to high-energy ionizing radiation, such as ultraviolet radiation, X-rays, and γ-rays.

The discovery and use of hybrid PAN-based materials and MOFs for CO_2 adsorption is relatively recent. While there has been considerable work on the CO_2 capture using MOFs,[87] crystalline MOFs possess fragility and tend to disintegrate into fine powders, leading to practical issues, such as pipe blockages, decreased gas separation efficiency, and material loss. Therefore, a strategy to address this challenge is creating MOF/polymer-fiber structures through electrospinning, which may increase flexibility and self-supported porous structures for CO_2 capture continuous process. Some examples of MOFs that are being growth seeded or coated onto PAN fibers and developed through electrospinning are UTSA-16 (Co) and UTSA-16 (Zn),[88] MIL-101 (Cr, Mg),[89] and ZIF-8.[90] Not only do these material perform high CO_2 adsorption capacities, stability experiments shows that these materials remained robust under humid air and acidic gases, and also possesses excellent recyclability during several adsorption–desorption cycles. In addition to developing MOF-PAN hybrid materials as fibers, there have also been reports of constructing them into MOF/PAN adsorbent beads for direct industrial use of enhancing CO_2 capture. MIL-101(Cr)@GO/PAN mm-sized beads preserved the porosity characteristics with superior CO_2 capture performance compared to the parent MOF and other moisture-stable MOFs (**Figure 6**a).[91] In another report, SIFSIX-3-Ni@PAN composite beads prepared by phase

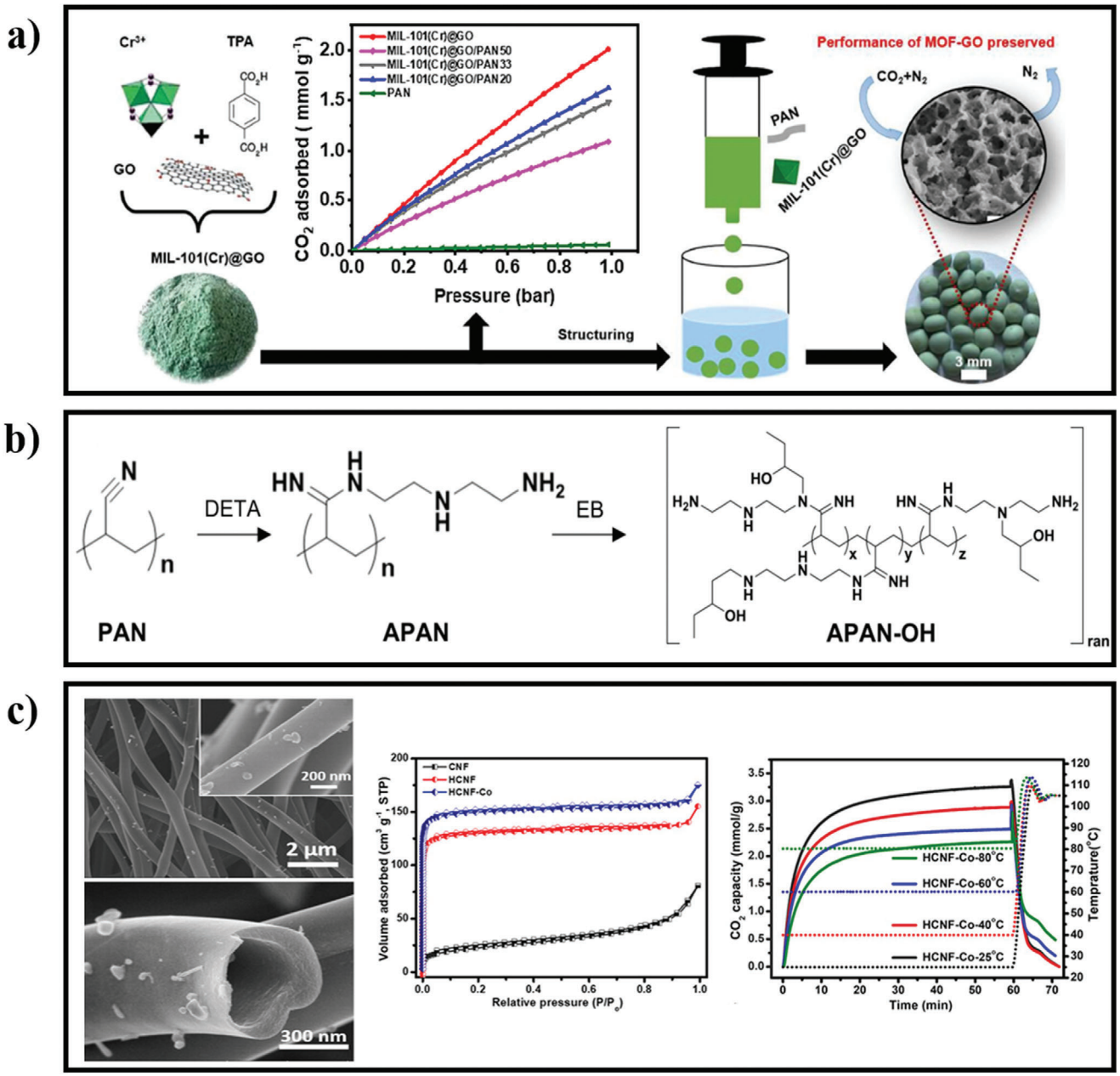

Figure 6. a) Fabrication route of MIL-101(Cr)@GO/PAN adsorbent beads and its CO_2 adsorption isotherm at 298 K. Reproduced with permission.[91] Copyright 2023, Elsevier. b) Schematic for the synthesis of APAN-OH nanoparticles from PAN. Reproduced with permission.[93] Copyright 2021, Elsevier. c) FE-SEM images, N_2 adsorption–desorption isotherms, and CO_2 capture of hollow PMMA/PAN CNFs hybridized with Co_3O_4 nanoparticles (HCNF-Co) at different temperatures. Reproduced with permission.[95] Copyright 2022, John Wiley and Sons.

inversion, demonstrated uniform MOF distribution in the porous structure with good mechanical stability and high CO_2 capacity, even at low CO_2 concentrations.[92] These MOF/PAN beads are suggested to pave the way for generating scalable and cost-efficient adsorbents, simplifying platforms for handling MOFs, and offer practical applications for CO_2 capture.

Reports of PAN itself being developed as nanoparticles and then surface-modified with alkylamine and sec-butanol, for achieving amine group stabilization under repeated CO_2 adsorption–desorption cycles, was described by Jung and co-workers.[93] They successfully designed mm-sized spherical adsorbents, namely APAN-OH and HPSA, with hierarchical pores via interconnecting the amine-rich nanoparticles. The schematic for APAN-OH synthesis from PAN is shown in **Figure** 6b. The inclusion of nanoparticles in PAN CNFs has also been studied as an alternative approach to improve CO_2 capture performance. Embedded SnO_2 nanoparticles were reported to enhance roughness, surface area, and flexibility of porous hollow PAN/polyvinylidene fluoride (PVDF) core–shell nanofibers, by acting as a plasticizer for single-fiber-crack connection, while also

offering additional vacant oxygen sites to enhance CO_2 adsorption capacity.[94] An even higher CO_2 uptake and CO_2/N_2 selectivity was demonstrated by polymethylmethacrylate (PMMA)/PAN core–shell nanofibers hybridized with Co_3O_4 nanoparticles, denoted as HCNF-Co, which also resulted in porous, hollow, flexible, and thermostable CNFs applicable as solid adsorbents for CO_2 capture (**Figure** 6c).[95] Another interesting strategy is the encapsulation of liquid-like nanoparticle organic hybrid materials (NOHMs) within submicron-scale PAN/ceramic electrospun fibers.[96] The bulk NOHMs, containing a silica core with ionically grafted branched PEI, were distributed near-uniformly throughout the superhydrophobic PAN/ceramic fibers, demonstrating high CO_2 capture kinetics practical for DAC.

In membrane separation for CO_2 capture, PAN is utilized mostly as a microporous support to a gutter layer. The gutter layer provides a uniform and highly permeable base for applying an ultrathin selective layer which helps to minimize the loss of gas permeance while preserving gas selectivity. Han et al. reported a novel fabrication method that enables precise control over thickness, yielding ultrathin gutter layers with uniform CO_2 permeance.[97] In their work, Polyactive (PA) selective layer was spin-coated onto crosslinked polydimethylsiloxane (PDMS) gutter layers on PAN substrates, achieving the highest ever reported CO_2 permeance of 3555 GPU and CO_2/N_2 selectivity of 40 (0.5 feed gas pressure at 35 °C) for a PA ultrathin film composite (UTFC) membrane. Notably, their method successfully obtained defect-free membranes with high repeatability of ultrathin PDMS gutter layer (98.4% success rate) and excellent CO_2 separation performance that falls within the specified range intended for economical utilization in postcombustion processes. Selyanchyn and co-workers[98] deposited Pebax-1657 ultrathin selective layer onto the surface of PDMS gutter layer activated by oxygen plasma. This double layered structure was then applied onto the PAN support. The report suggests that the oxygen plasma-controlled nanoblending at the interface between the selective and gutter layers of the TFC were pivotal in improving CO_2/N_2 selectivity to reach up to 72, surpassing the separation capability of the pristine Pebax-1657 polymer.

In another report, the addition of Cu-BDC MOF nanosheet layers onto PDMS/PAN membranes has been described by Sabetghadam et al.[99] The MOF nanosheets were discovered to be covering defects during the thin membrane formation, rendering a gutter layer unnecessary, and enhancing the CO_2/N_2 selectivity up to 77. A different approach to develop mechanically robust composite membranes was proposed by Sun and co-workers.[100] In their work, PAN was developed as electrospun nanofiber mat (NFM) and then low molecular weight polyethylene glycol (PEG) was interpenetrated into the inner-voids of PAN NFM via in situ photopolymerization to construct defect-free poly(ethylene oxide) (PEO)/PAN nanofiber composite membranes (NFCMs). The process was mimicking "reinforced-concrete," in which the PAN nanofiber and PEO matrix were bonded through adhesive force to withstand external forces collectively, creating nanofibers interpenetrating network that leads to elevated mechanical properties. The obtained NFCMs exhibited high CO_2 permeability of 343 Barrer and CO_2/N_2 selectivity of 65.4, transcending the 2008 Robeson upper bond. Later on, this procedure was modified by growing ZIF-8 MOF crystal seeds on the surface of PAN NFMs that acts as a skeleton, before the in situ photopolymerization of PEG to construct ZIF-8@PAN/PEO MMCMs.[101] The findings indicate that the MOFs-modified PAN/PEO membranes exhibit a slight decrease in CO_2/N_2 selectivity but better mechanical strength compared to PEO/PAN membranes, suggesting it to originate from the enhanced interaction between the nanofibers and the PEO matrix induced by the ZIF-8 growth.

2.2. Synthetic Porous Organic Polymers (POPs)

Another approach to enhance CO_2 capture is to increase the surface area of sorbents using porous materials. POPs represent a developing category of porous materials, made of organic and lightweight components linked by strong covalent bonds. POPs display a range of beneficial properties, such as low density, large surface areas, tuneable pore sizes featuring various channels, and plenty of reactive functional groups. Additionally, they provide easily modifiable functionality, outstanding physicochemical stability, along with diverse design possibilities and synthesis methods.[7] Several types of POPs have been reported in the literature. Among them, conjugated microporous polymers (CMPs), hyper-crosslinked polymers (HCPs), and covalent organic frameworks (COFs) have been widely employed for CO_2 capture. Herein, we have outlined the latest advancements of CMPs, HCPs, and COFs within the past 5 years.

2.2.1. Conjugated Microporous Polymers (CMPs)

CMPs are 3D semiconducting polymers in which rigid aromatic groups are interconnected, either directly or through double or triple bonds, creating π-conjugated microporous networks, and offers useful electronic properties. In nearly all cases to date, the covalent bonds in CMPs are formed irreversibly, and the polymerization follows a kinetic pathway. As a result, all CMPs (apart from any conjugated covalent organic frameworks (COFs)) are amorphous.[102] The first examples of CMPs were reported by Jiang et al. in the synthesis of conjugated microporous poly(aryleneethynylene) networks formed by Sonogashira–Hagihara cross-coupling reaction of alkynyl arene monomers linked with halogen-containing aromatic compounds.[103] Its Brunauer–Emmett–Teller (BET) surface area reached 834 $m^2 g^{-1}$ and later was found to exhibit CO_2 sorption capacities of 0.97 mmol g^{-1} at 298 K and 1 bar.[104] Since then, new designs and synthetic routes of CMPs were established via a wide range of coupling reactions, including the Sonogashira–Hagihara coupling reaction,[103] Suzuki–Miyaura coupling reaction,[105] Yamamoto coupling reaction,[106] Heck coupling reaction,[107] cyclotrimerization reactions,[107] phenazine ring fusion,[107] Schiff-base condensations,[108] heterocycle linkages,[102] alkyne metathesis,[102] oxidative coupling,[102] Buchwald–Hartwig amination,[102] electropolymerization,[102] and hypercrosslinking linear conjugated polymers.[102]

Typically, CMPs are synthesized using diverse Pd-catalyzed C—C coupling reactions. Ren et al. successfully homocoupled 1,3,6,8-tetraethynylpyrene using a Pd(II)-Cu(I) catalyst to afford a highly conjugated microporous polymer.[109] The 1,3-diyne-linked CMP exhibited excellent selectivity of CO_2/N_2 of 44.2 and CO_2/CH_4 of 8.2 with good thermal stability and high isosteric heats of CO_2 adsorption confirmed by the IAST. Wang and

co-workers developed a series of thiophene- and nitrogen- rich CMPs, namely SNCMP-1 and SNCMP-2, via a Pd(II)-catalyzed coupling reaction which demonstrated superior CO_2 adsorption capacities up to 3.894 mg g^{-1} at 70 bar and 323 K.[110] In addition to Pd(II), the utilization of other metal catalysts is also reported on the synthesis of N-rich triazine-based CMPs. A novel oxidative copolymerization reaction in the presence of iron(III) chloride was performed to obtain poly(triazine-*co*-pyrrole)-based CMPs.[111] Good thermal stability and high BET surface area was achieved for the denoted TP-CMPs, which facilitated good CO_2 adsorption of up to 1.09 mmol g^{-1} at 298 K (1 bar). In another report, Qiao et al. utilized the Lewis acid zinc chloride ($ZnCl_2$) to obtain a series of triazine-based CMPs with good porosity and high CO_2 adsorption capacity up to 120.8 cm^3 g^{-1} at 273 K and 1 bar.[112] To summarize, based on both experimental and theoretical investigations to date, the design of CMP with favorable CO_2 capture properties typically concentrated on i) achieving high BET surface area and porosity,[111] ii) incorporating polar units into the CMP framework to enhance adsorption sites, including carboxylic acids, amines, hydroxyl groups, sulfur, etc.,[113] and iii) employing postsynthetic amine functionalization.[114]

The residue of the metal catalyst, mostly Pd(II), are often persistently present within the polymers and the challenges associated with complete removal, significantly impedes the elucidation of structure–property relationships of CMPs. Therefore, recently the synthesis of CMPs are more likely performed without the use of metal catalysts. An elegant synthesis of CMP employing organic acids as the catalyst, which facilitated easier removal of catalyst residues, was reported by Cheng and Han.[115] In their work, they have designed rich oxygen atom-decorated CMPs, referred as O-CMPs, through aldol condensation of *s*-indacene-1,3,5,7(2*H*,6*H*)-tetrone and different types of aromatic aldehydes to afford the highest CO_2 uptake of 4.36 mmol g^{-1}, facilitated by quadrupole interactions. Another example of avoiding the use of Pd(II) catalyst in CMPs synthesis was reported by Meng and co-workers.[116] Their synthetic strategy successfully obtained two metal-free redox-active truxene-based CMPs linked by fused heterocyclic thiazolo[5,4-*d*]-thiazole moieties, namely Tx-TzTz-CMP-1 and Tx-TzTz-CMP-2, which exhibits high BET surface areas and CO_2 uptakes. **Figure 7** shows how the N-sites (tertiary amines), which facilitated the enhanced CO_2 uptake, are incorporated into the porous materials of Tx-TzTz-CMP-1 and Tx-TzTz-CMP-2 via condensation reactions of the aromatic aldehydes and dithiooxamide (DTA). N_2 sorption isotherms and CO_2 adsorption isotherms of the materials are also displayed. Subsequently, the two CMPs were further employed as metal-free photocatalysts for the photoreduction of CO_2 to CH_4 under visible light exposure.

2.2.2. Hypercrosslinked Polymers (HCPs)

HCPs are amorphous materials formed typically by the Friedel–Crafts alkylation chemistry of aromatic polymers and monomers in halogenated solvents. The small volume of aromatic rings enhances the possibility of the monomers involved in the Friedel–Crafts reaction allowing additional crosslinking nodes.[117] Therefore, extensive crosslinking through methylene bridges in HCPs result in elongated polymers with very high surface area and permanent microporosity (d < 2 nm), even after solvent is removed.[118] The microporosity of HCPs relies on the degree of crosslinking, which can be adjusted by selecting substrates and solvents, using external crosslinking agents, and employing various chemical methods.[119] Other notable advantages of HCPs are their moderate synthesis requirements, easy functionalization, adaptable structures, as well as their excellent physical and thermal stability. Additionally, HCPs serve as cost-effective options for large-scale applications because of the abundance of low-cost raw materials.[120] There are three approaches available for producing HCPs: i) the one-step polycondensation of functional monomers or internal crosslinking, ii) external crosslinking of rigid aromatic structural blocks, and iii) the post-crosslinking of polymer precursors.[121] Davankov et al. introduced HCP for the first time, featuring a higher degree of crosslinking (exceeding 40%) compared to commercial crosslinked polystyrene (PS), hence earning the designation of hypercrosslinked PS or Davankov-type resin.[122] Since then, studies of HCPs have garnered great attention especially for its potential application in CO_2 capture as porous solid sorbents.

Enhancement of HPCs' CO_2 uptake can be achieved by chemical modifications to improve the electrical properties of HPCs surface, such as dipole moment and polarizability. Amine grafting into benzene-based HCP networks has been reported by Moradi et al.[118] **Figure 8a** illustrates the incorporation of primary amine into the porous HCP network and its selective CO_2/N_2 adsorption behavior. The findings, as displayed in **Figure 8a–d**, show that after amination, the BET surface area and pore size decreased, while the CO_2 uptake capacity increased from 301.67 to 414.41 mg g^{-1} as well as obtaining 43% enhancement of CO_2/N_2 selectivity. Torkashvand et al. reported amine grafting on carbazole-based HCPs, namely NH_2-HCPs.[123] Similar to previous findings, the BET surface area of these materials reduced from 705.35 to 471.21 m^2 g^{-1}, while enhancing the CO_2 capacity to 236.37 mg g^{-1}. Decrease of BET surface areas could be attributed to the occupation of pores by the amine groups, nonetheless, the increase in adsorption capacity resulted from the addition of amine functional groups. Teng and co-workers fabricated naphthalene-based HCPs via a simple one-pot external crosslinker knitting method followed by N-impregnation which featured high surface area and high CO_2 uptake up to 3.8 mmol g^{-1}.[124] The N-doping of HCPs through impregnation increases the basic N moieties in the porous networks, enhancing the Lewis acid-base interaction of adsorbents and CO_2.

Nonionic HCPs possess few active functionalized sites, which limits their potential applications in CO_2 conversion. Thus, to enhance their capabilities, ILs are introduced into porous HCPs to create hypercrosslinked ionic polymers (HIPs). These HIPs combine the benefits of HCPs and ILs. The large surface area and high microporosity of HCPs facilitate efficient CO_2 capture, while ILs offer catalytic active sites for CO_2 conversion. This approach represents the alternative for metal-free heterogeneous catalysts in CO_2 cycloaddition, avoiding the energy-intensive process for recovering the co-catalyst and environmental pollution by the leaching of metals. Generally, HIPs are primarily synthesized through the crosslinking of ionic and neutral monomers, the in situ generation of ionic sites during hypercrosslinking, and postfunctionalization strategies.[125] To date, numerous HIPs materials have been synthesized for CO_2 capture and

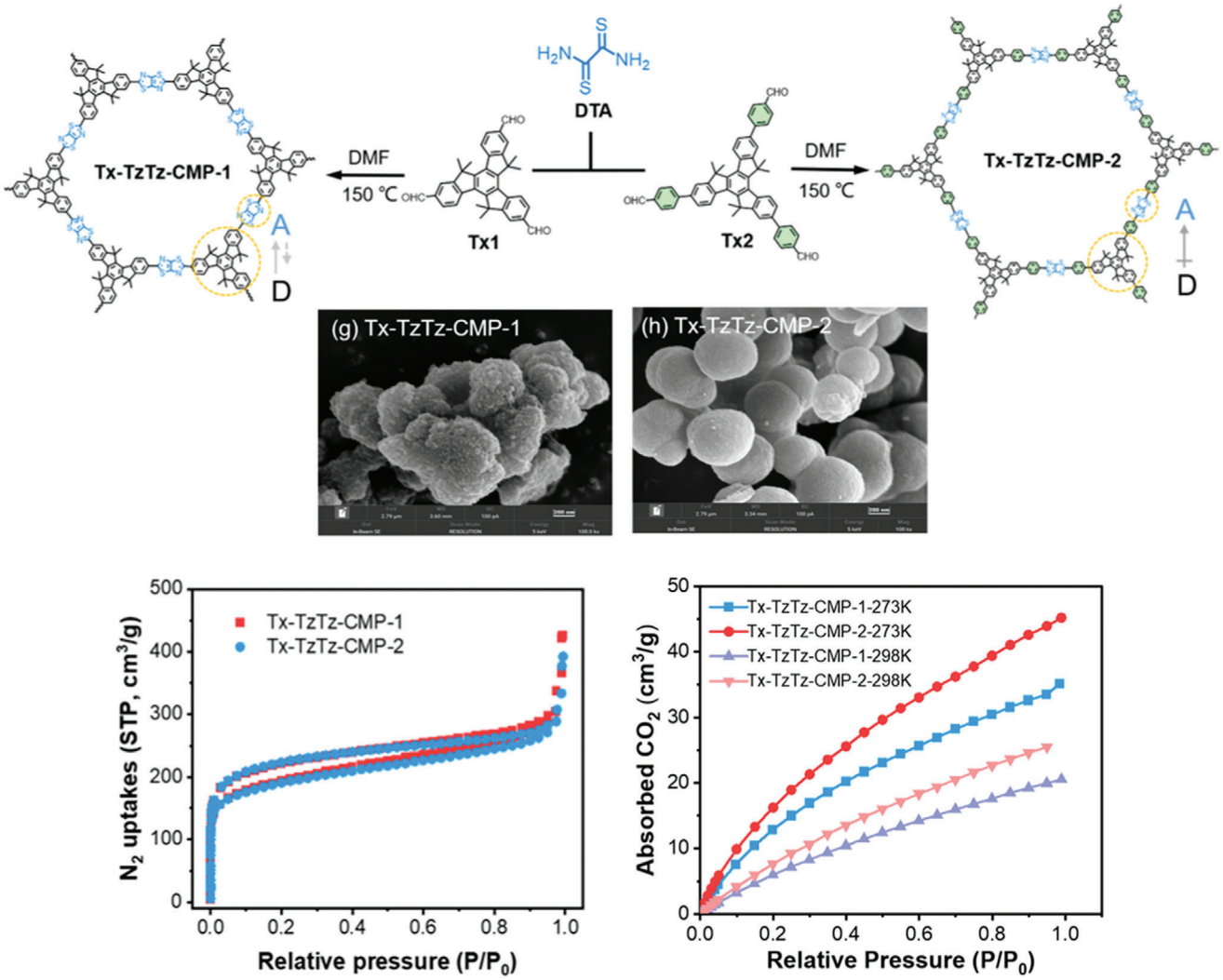

Figure 7. Synthesis of Tx-TzTz-CMP-1 and Tx-TzTz-CMP-2, their SEM images, N_2 sorption isotherms, and CO_2 adsorption isotherms at 273 and 298 K. Reproduced with permission.[116] Copyright 2023, American Chemical Society.

conversion. Liao and co-workers[125] developed a novel systematic postsynthetic modification strategy to synthesize imidazolium-based HIPs with elevated ionic content up to 2.1 mmol g^{-1} and a substantial specific surface area of 385 m^2 g^{-1} from porous HCPs through addition reactions and quarternization. The resultant HIPs demonstrated good CO_2 uptake, outstanding catalytic yields, reusability, and stability. Xu et al. reported a successful synthesis of aluminum-porphyrin-based HIPs (Al-HIPs) using the direct knitting approach by employing low-cost metalloporphyrins and selected ILs for the first time.[126] By introducing the 3D tetraphenylmethane fragments, the crosslinking sites increased, improving the reactivity ratios of the ILs in the polymerization process. Concurrently, integrating imidazolium-based ILs as flexible pendant chains onto the porphyrin backbones, connected by methylene groups, may address the limitation of Friedel–Crafts alkylation for electro-deficient aromatic monomers while enhancing the stability of metal active species. The obtained HIPs exhibited high surface area up to 432 m^2 g^{-1} and stronger CO_2 uptake up to 2.10 mmol g^{-1} at 273 K and 1 bar.

The recent encouraging advancements in HCPs are directing research toward more environmental-friendly materials and sustainable synthesis methods. Green materials, such as lignin-[127] and histidine-based HCPs,[128] have been reported as adsorbents for efficient CO_2 capture. An alternative of using waste materials, such as waste Styrofoam (the tradename for expanded polystyrene) is also another strategy being explored.[119,129] Chanchaona and Lau assessed how changing the reactor type could impact the environmental footprint and sustainability of HCP synthesis.[121] In their work, poly-α,α'-dichloro-*p*-xylene HCPs, namely *p*-DCX, *p*-PS-DCX, and *p*-PS-FDA, were synthesized by both, batch- and continuous flow synthesis, each using the three approaches of crosslinking (**Figure** 8e). The results of the life-cycle assessment (LCA) showed that compared to the traditional batch method, continuous flow synthesis offers a greater reduction in environmental impacts when post-crosslinking was applied, followed by external crosslinking, and finally internal crosslinking. The product yield was identified as key for promoting this environmental sustainability and by considering its

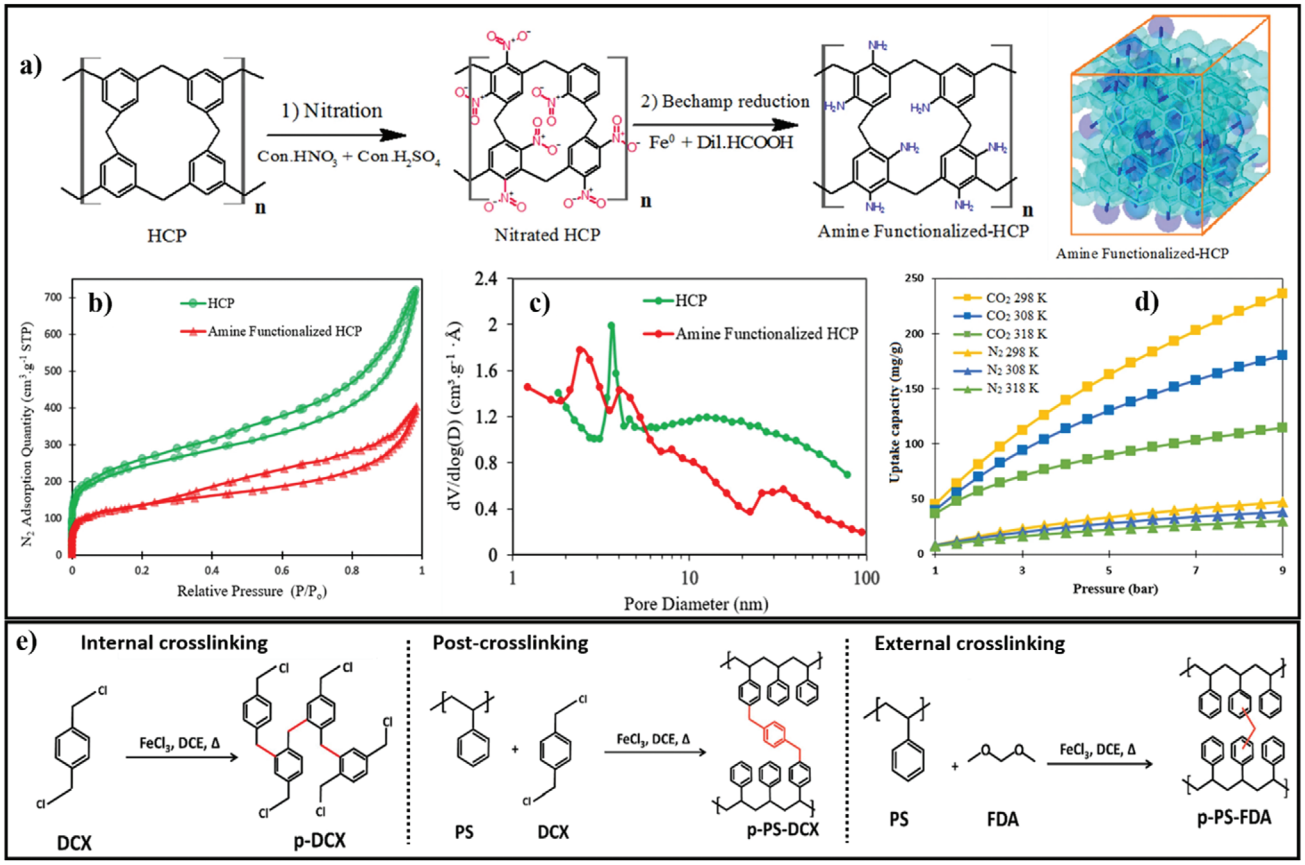

Figure 8. a) Synthesis of amine-functionalized HCP. b) N_2 adsorption–desorption isotherms of HCP and amine-functionalized HCP. c) Pore size distribution curve by BJH method, and d) selective adsorption behavior of amine-functionalized HCP at CO_2/N_2 composition of 15:85. Reproduced under terms of the CC-BY license.[118] Copyright 2023, Moradi, M. R. et al., published by Springer Nature. e) Three synthetic crosslinking approaches of *p*-DCX, *p*-PS-DCX, and *p*-PS-FDA HCPs for LCA study. Reproduced with permission.[121] Copyright 2023, Elsevier.

benefits including reduced environmental impact, superior CO_2 capture performance, and increased productivity, they suggest that continuous flow synthesis should be extensively adopted for scaling up HCPs production in industrial settings.

2.2.3. Covalent Organic Frameworks (COFs)

COFs are porous crystalline materials assembled by lightweight elements, uniform nanopores and structured frameworks, comprised of organic building blocks linked by robust covalent bonds via a range of reversible reactions.[130] COFs are metal-free and nontoxic in nature. Additionally, due to their precise functionalities and predesigned structures, they attain excellent selectivity toward guest molecules.[131] Their ordered pore distribution features, straightforward pore surface engineering, low regeneration energy requirements, and excellent stability,[132] enables chemical and structural control tailored to specific functions, such as gas adsorption. In terms of CO_2 capture materials, a thorough review specifically on COFs have been made by Zhao et al.[133] Their review includes several organic reactions that have been employed to synthesize COFs materials, such as the formation of B—O (boronate, boroxine, and borosilicate), C═N (imine, hydrazine, and squaraine), C—N (triazine and imidization), B—N (borazine), and N—N (azodioxides) bond linkages. In the past 5 years, COFs are the most popular studied among all porous organic polymers based on the number of articles and reviews published.

Following its initial discovery by Yaghi et al. in 2005,[134] a significant number of 2D COFs for CO_2 capture were reported. A stable 2D hydrazone-linked COF, namely TPT/OH, was synthesized under solvothermal conditions to attain highly crystalline and N-rich porous structure with a periodic hexagonal order.[131] The TPT/OH presented high surface area and high average pore size, with effective CO_2 capture of 0.9 mmol g^{-1} at 1 bar and 298 K. An alternative CO_2 capture mechanism utilizing metal ion-doped Schiff base imine 2D COFs as adsorbents was proposed by Kang et al.[135] In this capture mechanism, CO_2 molecules insert between the metal ion and the N atom of the imine bond on the inner pore surface of the COFs. This results in unconventional sorption isotherms that are characterized by tunable adsorption steps and enhanced CO_2 sorption capacity. Consequently, the CO_2 adsorption capacity of the ion-doped Py-1P COF is enhanced by 89.5% in comparison to that of the undoped Py-1P COF.

2D triazine-based COFs, or commonly known as covalent triazine frameworks (CTFs) have also been reported in recent works. The CTFs are nitrogen-rich frameworks, constructed by

aromatic 1,3,5-triazine rings.[136] CTFs demonstrate high CO_2 capacity and selectivity, along with optimal isosteric heat of adsorption (Q_{st}) for regeneration. They maintain their high CO_2 capture performance through multiple regenerations, even in the presence of water vapor, making them excellent candidates for CO_2 capture.[133] Kumar et al. reported on the synthesis of a 2D CTF, namely IITR-COF-1, via the polycondensation of 2,4,6-tris(4-formylphenoxy)−1,3,5-triazine with a triamine linker.[137] The CTF exhibited superior BET surface area of 2830 $m^2\ g^{-1}$ and an exceptional CO_2 capture capacity of 131.9 cc g^{-1} (25.9 wt%) at 273 K and 1 bar. Zhao et al. developed a (3,3)-connected triazine-based COF, denoted as COF-Z1, by a solvothermal method, that demonstrates good CO_2/N_2 adsorption selectivity of 35.09 at 273 K.[138] A maximum CO_2 adsorption capacity of 24.21 (21.38) $cm^3\ g^{-1}$ at 273 K was achieved, with a moderate Q_{st} value of 20.31 kJ mol^{-1}, indicating that the CO_2 adsorption follows physisorption which is suitable for recycling and reuse.

2D COFs featuring with pore sizes larger than 8 Å, often are unsuccessful in achieving significant enhancement in gas separation selectivity via molecular size sieving. In contrast to traditional 2D COFs, formed from planar monomers, 3D COFs that are assembled from 3D building blocks are more likely to possess complicated porous structures with high crystallinity.[139] The synthesized 3D azine-linked 3D COF (3D-HNU5) has a twofold interpenetrated diamond topology that exhibits narrow pore size distribution, excellent thermal, and chemical stability, with high selective uptake of CO_2 over N_2 and efficient catalytic activity under mild conditions.[140] In another work, crystalline isostructural porous cage 3D-OC-COFs were successfully assembled utilizing a flexible prism-like building block ($6NH_2$-OC.4HCl) and an innovative in situ acid-base neutralization approach.[141] By strategically introducing various substituents into the initial dialdehydes during the assembly process, network conformations can be fine-tuned, leading to the formation of one expanded structure (3D-OC-COF-H) and two distinct contracted structures (3D-OC-COF-OH and 3D-OC-COF-Cl). Among all of these 3D cage-based COFs, 3D-OC-COF-OH performed the best CO_2/CH_4 separation performance.

The incorporation of specific polar groups into COFs enhances the effective interactions with CO_2 molecules, thereby providing an effective strategy to increase CO_2 uptake at low pressure.[131] Lyu et al. demonstrated that such a COF functionalized with polar amine groups enables it to capture CO_2 from dry air.[142] **Figure 9a** illustrates the synthetic scheme of the aforementioned COF, denoted as COF-609, which was made through crystallization of an imine-linked backbone, then followed by an aza-Diels-Alder cycloaddition, and finally by amine-functionalization. **Figure 9b** clearly displays how the amine groups incorporate into the framework. Results show that the attained COF-609 exhibited a 1360-fold increase in uptake capacity, when compared to the pristine framework. Moreover, in the presence of humidity, there is a further 29% increase in uptake capacity, meaning that there is potential for COF-609 to be used for DAC of CO_2 (**Figure 9c**). Wei and co-workers investigated four functionalized 3D COF-300s (COF-300-X, where X = $-SO_3H$, $-NO_2$, $-OH$, and $-NH_2$) for CO_2 adsorption and separation.[143] These findings suggest that functionalization substantially enhances the CO_2 adsorption capacity within the COF-300s. Notably, the top-performing COF-300-SO_3H exhibits an exceptional CO_2 adsorption capacity of 6.23 mmol g^{-1} and a high CO_2/N_2 selectivity of 393 at 298 K and 100 kPa. All of the functionalized COF-300s offers a conducive environment for CO_2 adsorption, characterized by a high accessible surface area, appropriate pore size, and significant porosity.

A straightforward method for synthesizing COFs, involves the Schiff base condensation reaction; for example reaction of triformyl-resorcinol and phenylenediamine in solvothermal conditions to produce 2D IISERP-COF15 was performed by Chakraborty et al.[144] The material attained moderate CO_2 uptake of 2.5 mmol g^{-1} at room temperature and increased to 15 mmol g^{-1} at 195 K. Introducing heteroatoms onto the pore-walls of mesoporous COFs provides space for anchoring/growing catalytic nanoparticles. Therefore, with this knowledge, and realizing that the neat COF did not catalyze CO_2 fixation, Ag nanoparticles (≈4–5 nm) were grown onto the COF to form Ag@COF. This modified COF, catalyzes the conversion of propargyl alcohols to alkylidene cyclic carbonates in the presence of CO_2, with good selectivity and an excellent yield of 90%. This finding confirms that modification of the COFs was crucial in capturing and activating CO_2 molecules. In order to investigate the relationship of COF structure and CO_2 capture performances, Wang and co-workers prepared a series of Schiff base COFs with different functionalities, pore sizes, and framework dimensions to undergo CO_2 capture performance and stability tests.[145] Their findings suggest that the two COFs with secondary amines resulting from enol-to-keto tautomerism, NUS-2 and TpPa-1, exhibit superior CO_2 capture performances compared to other imine COFs examined in this study. Both demonstrate room temperature dry CO_2 uptake capacities exceeding 0.5 mmol g^{-1} and CO_2/N_2 sorption selectivity of ≈30, also successfully maintained 70% of their dry CO_2 adsorption capacities under humid conditions (RH 17%). This can be attributed to the moderately hydrophobic pore environment of the COFs. Given the significant expense associated with flue gas desiccation, Wang and co-workers propose that COFs exhibiting moderate hydrophobicity hold potential as viable adsorbents for practical postcombustion CO_2 capture applications. Likewise, Zhang et al. described a novel microporous T-COF synthesized via a Schiff base reaction, demonstrated favorable thermal and chemical stability.[146] The synthesized T-COF displayed remarkable CO_2 capture capability, reaching up to 178 mg g^{-1} at 273 K. This high CO_2 capture capacity was credited to the microporosity of the structure and the presence of numerous active functional units anchored onto the skeleton.

In addition to their use as solid adsorbents for CO_2 capture, COFs have also been developed for use in membrane separation technology. In contrast to the inorganic–organic hybrid composition of MOFs, the purely organic composition of COFs may offer improved compatibility with polymers, potentially reducing the likelihood of forming defects at the interface between the polymer and filler during the preparation of MMCMs.[147] The first example of COF-based membranes for CO_2 separation was reported by Kang et al. in 2016.[148] The MMCMs were designed by exfoliating 2D COFs into nanosheets and then blended with commercial poly(ether imide) (Ultem) or polybenzimidazole (PBI). The resulting MMCM demonstrated excellent H_2/CO_2 permselectivity that surpassed the 2008 Robeson upper bound. Within the past 5 years, COF-based membranes for CO_2 separation have been developed with further modifications. Cheng et al. reported the effectiveness of 3D COF fillers in two different polymer

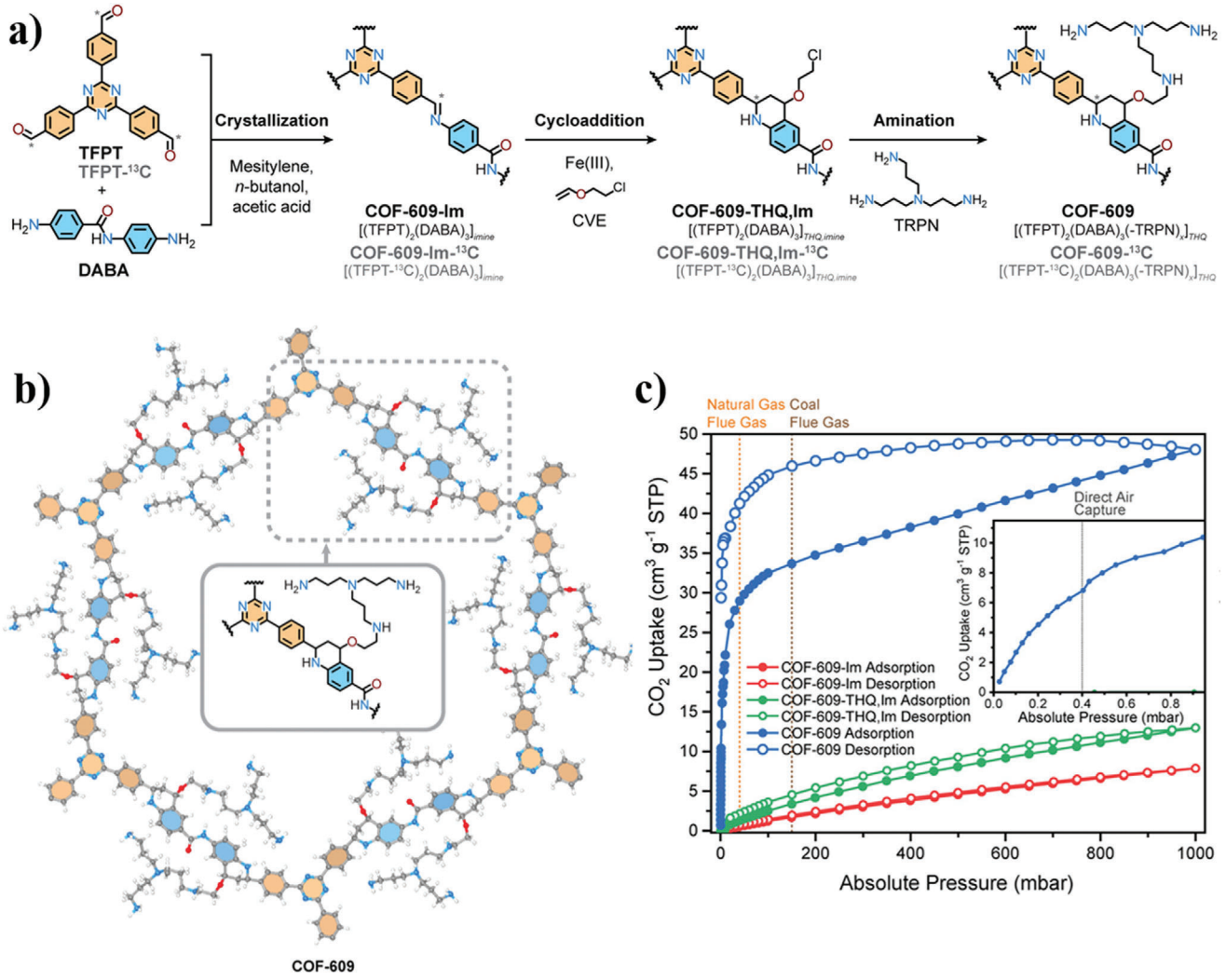

Figure 9. a) Synthetic scheme of COF-609. b) Structure of COF-609, and c) CO_2 isotherms at 25 °C. The inset in (c) shows a detailed view of the adsorption branch of COF-609 at 0–1 mbar to emphasize the uptake at pressures relevant to DAC. Reproduced with permission.[142] Copyright 2022, American Chemical Society.

matrix, glassy 6FDA-DAM and rubbery Pebax, to be fabricated as MMCMs.[139] The ultrasmall size-selective pores (4 Å) of these COF-300 fillers not only facilitates good polymer-filler interfacial compatibility, but also increases the membrane fractional free volume in order to achieve high permeability and gas pair selectivity. The 6FDA-DAM and Pebax MMM systems experienced an ≈52% and ≈57% increase of CO_2 permeability, respectively. Moreover, they attained high CO_2/CH_4 selectivity levels, reaching 75 and 110, respectively. Additionally, PEI functionalization was performed on the COF-300 by grafting onto the porous fillers. The COF@PEI-based MMCMs demonstrated significant CO_2/CH_4 and CO_2/N_2 selectivity improvements, even surpassing the Robeson upper bound. Regarding to its good polymer-filler compatibility, Xu et al. incorporated COFs (TpPA-1) with rich —NH— groups into polyamide (PA) segment through in situ interfacial polymerization to construct defect-free TFC membranes optimized for CO_2/N_2 separation.[149] The inclusion of COFs disrupts the rigid structure of the PA layer and augmented the quantity of effective carriers, creating fast CO_2 transfer pathways to boost CO_2 facilitated transport. As a result, the optimized TFC (TpPa0.025-PIP-TMC/mPSf) membrane demonstrated a high CO_2 permeance of 854 GPU and a high CO_2/N_2 selectivity of 148 at 0.15 MPa, with CO_2 permeance of 456 GPU and CO_2/N_2 selectivity of 92 at 0.5 MPa. In another report, Ying and co-workers successfully designed a series of ultrathin and oriented 2D COF films, notably COF-LZU1, with adjustable thickness to enhance overall CO_2 capture performance in TFC membranes.[150] They utilized this as a gutter layer to construct a thin photo-initiated crosslinked PEG (XLPEG) separation layer. Under optimized conditions, high CO_2 permeance of 1843 GPU and good CO_2/N_2 selectivity of 28.2 were attained, meeting the practical requirements of CO_2 performance target (CO_2 permeance > 1000 GPU and CO_2/N_2 selectivity > 20). Compared to other alternative gutter layer materials, COFs exhibit smaller and controllable transport resistance, offering insights for the development of next-generation CO_2 gas separation membranes.

Bora and co-workers, for the first time, employed a groundbreaking one-step approach, known as cold atmospheric plasma (CAP) treatment, for effective CO_2 gas adsorption.[151] The CAP treatment method not only achieves improved surface modulation of the membrane but is also the most straightforward, effective, and cost-efficient process operating under ambient conditions. The COF@PVDF membranes treated with CAP display a 36% enhancement in surface area and a 66% increase in CO_2 uptake, compared to the untreated membrane. The underlying reason for this derives primarily from the Lewis acid-base interaction between the electron-deficient carbon atom of CO_2 and the newly introduced functionalities on the surface of the COFs@PVDF membrane. The C—N bonds, characterized by higher electron density, are pivotal in facilitating this interaction. Most recently, Chang et al. modified TPB-DMTP-COF with an imidazolium-based [Emim][Tf_2N] IL and then prepared MMCMs by incorporating IL@COF into polymers of intrinsic microporous (PIMs).[152] PIMs is a class of polymers with microporous structure and high free volume. The IL modification not only improves the CO_2 affinity and reduces pore size of TPB-DMTP-COF but also enhances interfacial compatibility between PIM-1 and TPB-DMTP-COF. Consequently, introducing IL@COF into PIM-1 membranes enhances the CO_2/N_2 separation properties, with 3.0 wt% IL@COF/PIM-1 MMCMs exhibiting optimal CO_2 permeability and CO_2/N_2 selectivity of 9137.7 Barrer and 20.2, respectively, surpassing the 2008 Robeson upper bound. Furthermore, the resulting MMCMs demonstrate favorable continuous operation stability.

More recently, hybrid COFs with MOFs have been intensively studied for their enhanced CO_2 capture. Not only combining the advantages of MOFs and COFs, the hybrid MOF@COF also potentially enhance their performance synergistically at the MOFs-COFs interface. CO_2 uptake efficiency at low pressure (1 bar) is primarily influenced by the pore size rather than the surface area. Micropores, in particular, serve as the preferred sites for CO_2 adsorption, as they possess strong adsorption potential and can be substantially filled.[131] A novel covalently connected core–shell NH_2-UiO-66@Br-COFs hybrid material was synthesized through a Schiff-base reaction, in which Br-COFs shell was in situ grown on the NH_2-UiO-66 core.[153] The unique structure at the core–shell interface, which can be effectively adjusted by the coating of Br-COFs, yields abundant ultramicropores when compared to NH_2-UiO-66 and Br-COFs, with a maximum ultramicropore volume (V_{ultra}) of up to 0.157 $cm^3\ g^{-1}$. These ultramicropores at the core–shell interface significantly contributes to the CO_2 capacity, reaching up to 169.5 mg g^{-1} at 273 K and 1 bar, outperforming the corresponding single MOF and COF counterparts. Later on, this group reported COFs coating on Zr-MOFs, creating tunable micropores within the interface layer and ample N/S atoms for CO_2 capture.[154] The resulting bifunctional core–shell MOF@COF hybrid, referred to as M@COF-SF, demonstrates impressive BET surface area of 1301 $m^2\ g^{-1}$, a pore volume of 0.94 $m^3\ g^{-1}$, and heteroatom content of 13.38%. These attributes render its highly effective for CO_2 uptake, achieving 170 mg g^{-1} at 273 K and 1 bar.

The synthesis of hybrid COFs with ILs is also another approach to enhance the CO_2 capture performance of COFs. In a study reported by Xu et al., IL/ionic COF (ICOF) composites, synthesized in situ using a one-pot method within half an hour under ambient conditions, catalyze the cycloaddition reaction of CO_2 with epoxides to give cyclic carbonates.[155] These composites possess a favorable CO_2 adsorption capacity of 1.63 mmol g^{-1} at 273 K and 1 bar, while demonstrating exceptional catalytic performance in terms of both yield and durability. Yin et al. proposed an elegant synthesis to chemically integrate amino-functionalized imidazole IL (NH_2-IL) onto the channel walls of mesoporous COF of [HO]-TAPT-COFs to obtain [AeImBr]-TAPT-COFs (**Figure 10a**).[156] Due to the presence of amino polar groups and abundant imidazole cations of NH_2-IL along with its microporous nature, [AeImBr]-TAPT-COFs demonstrate enhanced CO_2 capture activity compared to its neat corresponding COF, increasing the CO_2 equilibrium capture capacity from 62.6 to 117.4 mg g^{-1} (**Figure 10b**), and demonstrating excellent CO_2/N_2 selectivity (**Figure 10c**). Additionally, the synergistic effect of $-NH_2$ and $-Br$ in NH_2-IL contributes to the improvement in the heterogeneous catalysis of CO_2-epoxide cycloaddition, yielding up to 99.1%, without the need for solvents and cocatalysts, and also performing excellent stability and cycle life. **Table 2** outlines CO_2 capture performances of all the reviewed POPs materials in this section, including CMPs, HCPs, and COFs.

2.3. Polymeric Membranes

The method that is best suited to capturing emissions from large stationary CO_2 sources is membrane-based separation. Different membrane separation scenarios are based on CO_2 concentration, pressure, separation specifications, and major contaminants of the applied source.[157] The membrane acts as a physical device that is able to remove one or more components selectively from a mixture. These membranes are highly attractive and energy efficient for CO_2 capture as they offer several advantages, such as their small size, operation and maintenance simplicity, compatibility, diversity, and lack of pollutant by-products.[158] One of the most commonly utilized material for this membrane separation method is the polymeric-based membrane.

In the postcombustion carbon capture, the CO_2 partial pressure is low and the flue gas is a mixture of gases; CO_2, N_2, O_2 as well as trace amounts of SO_x and NO_x, additionally water is present. Therefore, it is important for the polymeric membrane to have both high permeability and adequate selectivity toward CO_2 in order to attain deep carbon cleaning during this process.[159] However, it is well-known that a trade-off between permeability and selectivity exists for polymeric membranes[160] as defined by the Robeson upper-bound.[161]

It is of interest to design new types of polymers with ideal properties of permeability and selectivity to overcome the Robeson upper-bound and consequently strengthen the research field of composite membranes in CO_2 gas capture and separation. The polymers that are developed must also possess other ideal membrane criteria for CO_2 capture such as thickness, cost-effective, reproducibility, plasticization resistance, chemical, mechanical, physical, and thermal stability for industrial applications.[69,162] The first copolymer-based composite membrane material for CO_2 gas separation was patented by Blume and Pinnau in 1990.[163] This type of membrane exhibited a well-defined structure, enhancing gas transport pathways, which contributes to higher permeability and selectivity. Additionally, both thermal

Table 2. POPs and their features for CO_2 capture.

Strategy	Material	BET Surface Area [$m^2\ g^{-1}$]	Total Pore Volume [$cm^3\ g^{-1}$]	CO_2 capacity	Selectivity		Q_{st}[a] [kJ mol^{-1}]	Refs.
					CO_2/N_2	CO_2/CH_4		
CMPs								
Pd(II)-catalyzed oxidative homocoupling	LKK-CMP-1	467	0.371	9.78 wt% (273 K, 1 bar)	44.2	8.2	35.0	[109]
Pd(II)-catalyzed coupling; thiophene- and nitrogen-rich CMPs	SNCMP-1 SNCMP-2	16.1 41.7	0.22 0.54	3,894 mg g^{-1} 3,878 mg g^{-1} (all at 323 K, 70 bar)				[110]
Fe(III)-catalyzed oxidative copolymerization; triazine-pyrrole-based CMPs	TP-CMP-1 TP-CMP-2 TP-CMP-3	473.77 556.58 17.896	0.2678 0.2897 0.0727	1.05 mmol g^{-1} 1.09 mmol g^{-1} 0.71 mmol g^{-1} (all at 298 K, 1 bar)				[111]
Zn(II)-catalyzed, mixed-linker strategy under ionothermal conditions; triazine-based CMPs	CMP@1 CMP@2 CMP@3	325 523 707	0.26 0.31 0.37	63.7 $cm^3\ g^{-1}$ 96.5 $cm^3\ g^{-1}$ 120.8 $cm^3\ g^{-1}$ (all at 273 K, 1 bar)			29.2 33.4 36.0	[112]
Acid-catalyzed aldol condensation; rich oxygen-decorated CMPs	O-CMP-1 O-CMP-2 O-CMP-3	340 427 393	1.16 nm[b] 1.09 nm[b] 1.03 nm[b]	3.02 mmol g^{-1} 3.42 mmol g^{-1} 4.36 mmol g^{-1} (all at 273 K, 1 bar)	In a range of 22–25 for all the O-CMPs		In a range of 20–27 for all the O-CMPs	[115]
Metal-free redox-active truxene-based CMPs via condensation reactions	Tx-TzTz-CMP-1 Tx-TzTz-CMP-2	654 676	1.0 nm[b] 1.3 nm[b]	≈35 $cm^3\ g^{-1}$ ≈45 $cm^3\ g^{-1}$ (all at 273 K)				[116]
HCPs								
Amine functionalized benzene-based HCP	HCP Amine Functionalized HCP	806 453	1.09 0.61	301.67 mg g^{-1} 414.41 mg g^{-1} (all at 298 K, 9 bar)	43% enhancement after amine functionalized			[118]
Amine grafted carbazole-based HCP	HCP NH_2-HCP	705.35 471.21	0.954 0.517	182.1 mg g^{-1} 236.4 mg g^{-1} (all at 298 K, 5 bar)				[123]
Polycyclic aromatic hydrocarbons-based HCPs and amine-impregnation	HCLP 1 HCLP 2 HCLP 3 HCLP 4	2870 688 64 65	1.09 0.53 0.32 0.30	3.8 mmol g^{-1} ≈3.0 mmol g^{-1} 1.7 mmol g^{-1} 0.45 mmol g^{-1} (all at 273 K, 1 bar)				[124]
Imidazolium-based HIP by Friedel-Crafts alkylation, addition reaction and quaternization	[HCP-CH_2-Im][Cl]−1	385	0.332	1.79 mmol g^{-1} (273 K, 1 bar)				[125]

(*Continued*)

Table 2. (Continued)

Strategy	Material	BET Surface Area [$m^2\ g^{-1}$]	Total Pore Volume [$cm^3\ g^{-1}$]	CO_2 capacity	Selectivity		Q_{st}[a] [kJ mol^{-1}]	Refs.
Aluminium-porphyrin-based HIPs with imidazolium-based Ils br direct knitting approach	Al-HIP-2 Al-HIP-3	51 432		1.54 mmol g^{-1} 2.10 mmol g^{-1} (all at 273 K, 1 bar)			57.2 30.3	[126]
Lignin-derived oxygen-rich HCPs by Friedel–Crafts alkylation	HCP1 HCP2 HCP3 HCP4 HCP5 HCP6 HCP1b	14.1 20.6 16.5 246.9 15.4 40.6 7.8	0.023 0.033 0.038 0.230 0.035 0.074 0.021	64.1 mg g^{-1} 44.5 mg g^{-1} 49.7 mg g^{-1} 48.7 mg g^{-1} 52.6 mg g^{-1} 53.3 mg g^{-1} 36.1 mg g^{-1} (all at 273 K, 1 bar)	68.1 256.6 32.7 56.8 31.6 61.9 32.8		41.2 44.2 27.7 36.2 33.9 46.5 38.2	[127]
One-pot copolymerization of histidine, quaternization, and Friedel–Crafts alkylation	HCP-Br HIP-Br-His HIP-Cl-His HIP-Br-Imi	1171 719 967 123	2.42 2.00 1.96 0.33	1.2 mmol g^{-1} 2.9 mmol g^{-1} ≈2.6 mmol g^{-1}	21–53			[128]
Waste Styrofoam-based HCP by Friedel–Crafts reaction, Fe(III)-catalyzed	WSHC	802.84	0.5758	11.05 mmol g^{-1} (298 K, 10 bar)				[129]
COFs								
2D hydrazone-linked COF via reversible condensation reaction under solvothermal conditions	TPT/OH COF	424	3.35 nm[b]	0.9 mmol g^{-1} (298 K, 1 bar)				[131]
Metal ion-doped Schiff-based 2D COF	Py-1P Py-1P-$FeCl_3$	1718 1230	2.2 nm 1.9 nm	0.72 mmol g^{-1} 1.21 mmol g^{-1} (all at 298 K, 800 mmHg)				[135]
2D covalent triazine frameworks (CTF)	IITR-COF-1	2830	1.7	131.9 (25.9) cc g^{-1} (273 K, 1 bar)			25.6	[137]
Triazine-based COF by solvothermal method	COF-Z1	512.523		24.21 (21.38) $cm^3\ g^{-1}$ (273 K, 1 bar)			20.31	[138]
PEI-functionalized 3D COF as fillers in MMMs	COF-300 COF@PEI	1209 1020	4.1 Å[b]	23.5 $cm^3\ g^{-1}$ 48.9 $cm^3\ g^{-1}$ (all at 273 K, 1 bar)	9.9 17.6	1.8 3.7	17.7 21.8	[139]
Azine-linked 3D COF	3D-HNU5	864 (eksperiment) 5161 (theoretical)	0.89; 1.01 nm[b]	123.1 mg g^{-1} (273 K, 1 bar)				[140]

(*Continued*)

Table 2. (Continued)

Strategy	Material	BET Surface Area [$m^2\ g^{-1}$]	Total Pore Volume [$cm^3\ g^{-1}$]	CO_2 capacity	Selectivity		Q_{st}[a] [kJ mol^{-1}]	Refs.
Tunable cage-based 3D COF via an in situ acid-base neutralization	3D-OC-COF-H	1143	10.5-11.4 Å[b]	89.2 $cm^3\ g^{-1}$			22.4	[141]
	3D-OC-COF-OH	923	6.5 Å[b]	54.5 $cm^3\ g^{-1}$				
	3DOC-COF-Cl	660	5.3 Å[b]	36.8 $cm^3\ g^{-1}$ (all at 273 K, 1 bar)				
Imine-linkage-based COFs via Diels-Alder cycloaddition, and covalent incorporation of aliphatic amine into COFs	COF-609-Im	724	37 Å[b]	0.024 mmol g^{-1}				[142]
	COF-609-THQ,Im			0.057 mmol g^{-1}				
	COF-609			1.29 mmol g^{-1} (all at 298 K, 40 mbar)				
Functionalized 3D COFs	COF-300-THF	1719.85	0.86	1.30 mmol g^{-1}	6		17.74	[143]
	COF-300-OH	1422.76	0.74	2.07 mmol g^{-1}	11		21.32	
	COF-300-NH_2	1353.24	0.73	1.87 mmol g^{-1}	10		20.92	
	COF-300-NO_2	919.34	0.58	4.25 mmol g^{-1}	31		27.77	
	COF-300-SO_3H	428.42	0.45	6.23 mmol g^{-1} (all at 298 K, 100 kPa)	393		39.71	
Resorcinol-phenylenediamine-based 2D COF, by Schiff-base condensation under solvothermal conditions	IISERP-COF15	1230	0.6332; 12 Å[b]	2.5 mmol g^{-1} (298 K, 1 bar)	65	9.3	33	[144]
Schiff-base COFs	TpPa-1	684	14 Å[b]	0.65 mmol g^{-1}	114		44.0	[145]
	NUS-2	697	8.1 Å[b]	0.68 mmol g^{-1}	41.2		38.0	
	ACOF-1	872	8.2 Å[b]	0.34 mmol g^{-1}	26.3		20.5	
	TAPB-PDA	1845	35 Å[b]	0.10 mmol g^{-1}	9.4		24.5	
	COF-LZU1	904	18 Å[b]	0.20 mmol g^{-1} (all at 298 K, 0.15 bar)	31		22.4	
Schiff-base COF	T-COF	587	0.64	178 mg g^{-1} (273 K, 1 bar)			18.9	[146]
Rich —NH— groups COF	TpPa-1	171.27	1.58 nm[b]	51.27 $cm^3\ g^{-1}$ (273.15 K, 1 bar)				[149]
IL-COF for MMCMs	TPB-DMTP-COF	2137.6	1.31	≈25 $cm^3\ g^{-1}$				[152]
	IL@COF	1701.8	0.79	≈30 $cm^3\ g^{-1}$				
	COF/PIM	911.4	0.48	(all at 298 K, 1 bar)				
	IL@COF/PIM	763.7	0.46					

(*Continued*)

Table 2. (Continued)

Strategy	Material	BET Surface Area [$m^2\ g^{-1}$]	Total Pore Volume [$cm^3\ g^{-1}$]	CO_2 capacity	Selectivity	Q_{st} [a] [kJ mol^{-1}]	Refs.
MOFs-COFs hybrid, Schiff-base reaction	NH_2-UiO-66	1044	0.468	149.5 mg g^{-1}	28.18	95.8	[153]
	Br-COF	787	0.528	50.0 mg g^{-1}	22.41	24.7	
	NH_2-UiO-66@Br-COF-1	772	0.516	84.8 mg g^{-1}	25.26	53.0	
		796	0.523	89.0 mg g^{-1}	27.00	55.4	
	NH_2-UiO-66@Br-COF-2	865	0.591	123.2 mg g^{-1}	24.92	79.7	
		966	0.655	169.5 mg g^{-1} (all at 273 K, 1 bar)	24.08	117.2	
	NH_2-UiO-66@Br-COF-3						
	NH_2-UiO-66@Br-COF-4						
MOFs-COFs hybrid	Zr-MOF	667	0.54	63.5 mg g^{-1}	32.3	26.6	[154]
	COF	1037	0.79	46.1 mg g^{-1}	42.6	32.6	
	COF-SF	1499	0.92	35.4 mg g^{-1}	49.6	6.3	
	COF-S_2F	1396	1.19	55.8 mg g^{-1}	32.3	20.3	
	M@COF	847	0.75	88.2 mg g^{-1}	36.8	33.8	
	M@COF-SF	1301	0.94	170.0 mg g^{-1}	49.4	39.4	
	M@COF-S_2F	1011	0.88	121.7 mg g^{-1} (all at 273 K, 1 bar)	21.5	31.2	
IL/ionic COF composite	C_4-IL/ICOF	53	1.35 nm [b]	1.63 mmol g^{-1}			[155]
	C_6-IL/ICOF	103	1.35 nm [b]	1.41 mmol g^{-1}			
	C_{10}-IL/ICOF	113	1.35 nm [b]	0.86 mmol g^{-1} (all at 273 K, 1 bar)			
Amino-functionalized IL-grafted COF	$[AeImBr]_{83\%}$-TAPT-COF	55	0.20	117.4 mg g^{-1}	45.3		[156]
	$[HO]_{100\%}$-TAPT-COF	1783	1.51	62.6 mg g^{-1} (all at 298 K, 1 bar)			

[a] Q_{st} = Isosteric heat of adsorption, calculated by the Clausius–Clapeyron equation; Selectivity were calculated from single gas sorption isotherms based on the Ideal Adsorption Solution Theory (IAST); [b] Pore size distribution calculated from nonlocal density functional theory (NLDFT).

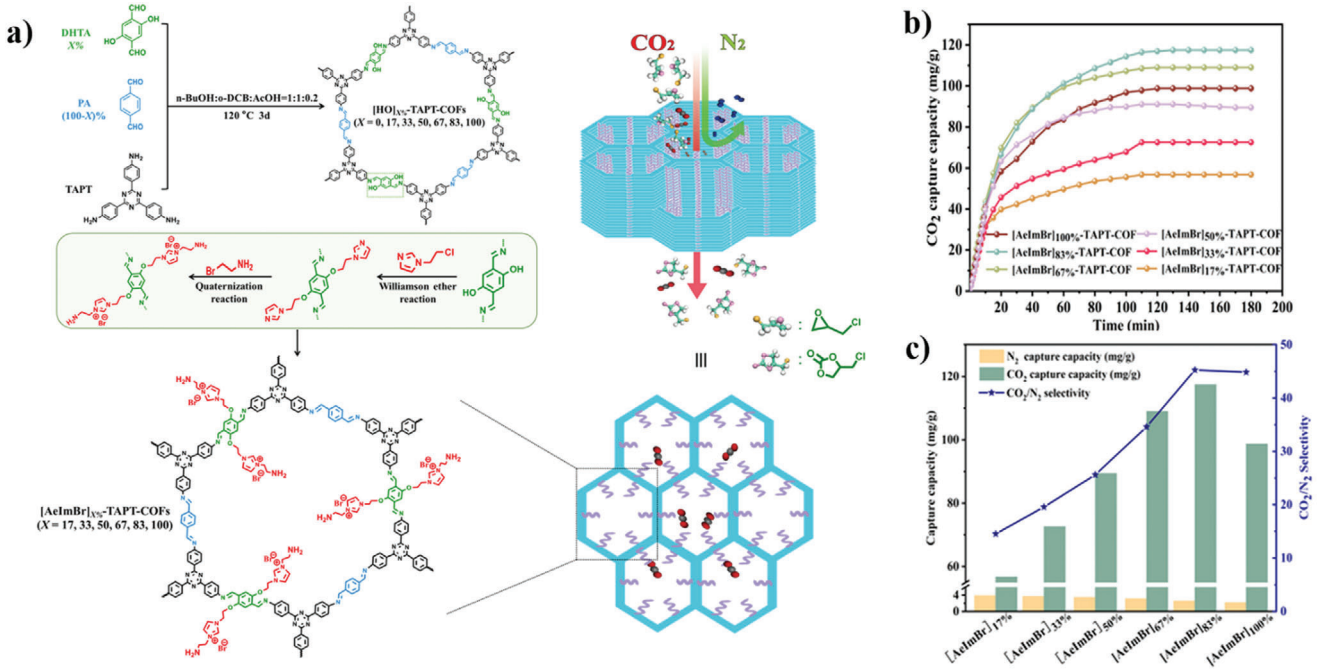

Figure 10. a) Schematic for the amino-functionalized IL/COFs of [AeImBr]-TAPT-COFs synthesis through a two-step modification method, b) CO_2 capture capacities of [AeImBr]-TAPT-COFs, and c) ideal CO_2/N_2 selectivity of [AeImBr]-TAPT-COFs. Reproduced with permission.[156] Copyright 2022, American Chemical Society.

and mechanical stability were observed over an extended period. Emerging polymeric membrane materials that have currently been studied for CO_2 capture are mainly based on the polymer-CO_2 interaction and polymer architecture. Some classes of these polymeric CO_2 membranes are ether oxygen-rich polymers, thermally rearranged (TR) polymers, perfluoropolymers, and facilitated transport membranes (FTMs).[157]

The polar ether linkage (—C—O—C—) in PEO is acknowledged for its strong affinity to CO_2 via quadrupole–quadrupole interactions. Nonetheless, a limitation arises from the tendency of polar ether groups to form strong hydrogen bonds with itself, leading to densely packed chains. The densely packed structures result in high crystallinity which is unfavorable for the fabrication of a defect-free membrane, as well as decreasing gas permeability. Therefore, various strategies have been employed to address this challenge. A green fabrication technique was proposed by Sun et al. to construct microstructural PEO membranes.[164] Large molecular-size bisphenol A ethoxylate diacrylate (BPA) was used to crosslink poly (ethylene glycol) methyl ether acrylate (PEGMEA) through rapid UV polymerization. The microstructure of membranes can be easily tailored by adjusting the ratio of the two prepolymers BPA and PEGMEA, with the aim to attain optimized microstructures with appropriate mesh size and PEO sol content. The resulted membrane addresses the trade-off challenge, by obtaining a CO_2 permeability of 1711 Barrer, a CO_2/N_2 selectivity of 44, and stable operation for 100 h under 15 atm. Another predominant method used to mitigate the high crystallinity of PEO involves block copolymerizing it with hard segments. The gas permeation characteristics of these copolymers are regulated by adjusting the lengths of the soft and hard segments, as well as modifying the proportion of the PEO phase within the copolymer. A block amphipathic copolymer, denoted as PDMS-b-PEO, was prepared by Liu and co-workers to be employed as an intermediate layer of an ultrathin Pebax and PAN membrane.[165] Pebax itself is a commercial PEO-based block copolymer made up of rigid polyamide blocks and soft polyether blocks, making Pebax less crystalline than the original PEO. The presence of PDMS-b-PEO in the intermediate layer enabled the successful fabrication of an integrated Pebax selective layer with a thickness of ≈50 nm. The resulting ultrathin Pebax composite membrane demonstrated remarkable performance, boasting a CO_2 permeance of 2142 GPU and a CO_2/N_2 selectivity of 36.[165]

TR polymers and polybenzimidazole (PBI) are emerging as potential candidates for precombustion processes among other polymer materials owing to their elevated H_2/CO_2 selectivity, moisture stability, and outstanding chemical resistance. Nevertheless, the pure PBI membrane shows limited H_2 permeability which is attributed to its densely packed polymer chains. Therefore, strategies for further enhancing H_2 permeability while preserving its selectivity are important for them to become more industrially attractive. A study by Moon et al. aimed to enhance the permeabilities of PBI-based membrane by mixing Celazole, a commercial PBI, with an *ortho*-functional PI, HAB-6FDA-Cl.[166] These blends undergo subsequent heat treatment to further augment their permeabilities, leveraging the thermal rearrangement reaction of *ortho*-functional polyimides, leading to the formation of polybenzoxazoles. In another study, PBI thin films were crosslinked with different concentration of 1,3,5-tris(bromomethyl)benzene (TBB) to tune polymer chain microstructure and fractional free volume (FFV) thus enhancing the sieving ability for H_2/CO_2 separation.[167] Gas separation tests conducted at 150 °C revealed that the membrane with the highest

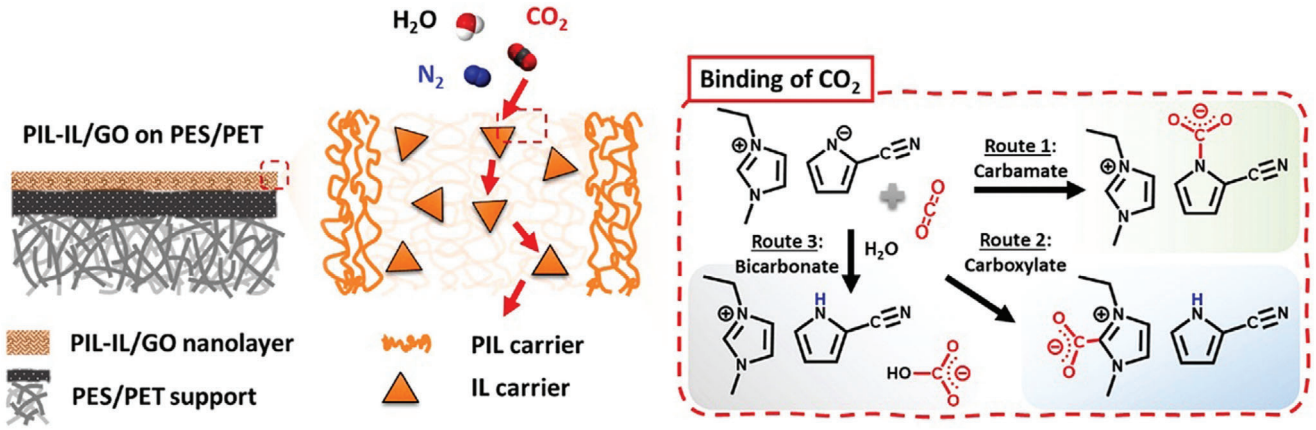

Figure 11. Illustration of the PIL-IL/GO membrane on PES/PET substrate and the CO_2 absorption reaction involving the IL mobile carriers. Reproduced with permission.[173] Copyright 2021, Elsevier.

crosslinking density and lowest FFV exhibited a H_2 permeability of 9.6 Barrer and remarkable H_2/CO_2 selectivity of 24, surpassing the Robeson upper bound.

Perfluoropolymers represent a category of glassy hydrocarbon polymers where most of the hydrogen atoms are substituted by fluorine atoms. Commercial amorphous perfluoropolymers, such as Teflon AF and Cytop, are recognized for their elevated gas permeability, which is attributed to the presence of pre-existing microchannels. Typically, these glassy polymers exhibit a selectivity favoring H_2 over CO_2 and CO_2 over CH_4. In the last 5 years, polytetrafluoroethylene (PTFE) in the module of hollow fibers have been mostly studied as membrane contactors[168] with superior CO_2 capture efficiency, reaching up to 99.3%.[169]

Another class of polymer with impressive selectivity and permeability of various gas pair is the thermostable polyimides (PI). Its commercially available form, Matrimid, has been extensively studied for membrane gas separation. Recent reports on Matrimid are to modify it with MOFs as nanofillers to be developed as MMCMs for energy-intensive gas separation processes. Bano and co-workers incorporated lanthanum (Ln)-MOFs in the Matrimid matrix to study selectivity and permeability of CH_4, CO_2, and N_2 gases through the resulted MMCMs.[170] It was shown that as the nanofiller loading in all MMCMs increased, CO_2 permeation improved significantly due to the porous nature of the nanofiller, introducing supplementary channels and FFV within the polymer matrix. Moreover, a higher nanofiller loading resulted in an increase in selectivity of MMCMs, rising from 34.1 to 48.45 for CO_2/N_2 and from 36.2 to 54.67 for CO_2/CH_4, which affirms the lack of membrane defects, enhanced filler/polymer interface, and good dispersion of the Ln-MOFs throughout the polymer matrix. Different loadings of a microporous 3D MOF, $Tb(BTC)(H_2O).(DMF)_{1.1}$, onto the Matrimid matrix was also reported for exhibiting good separation that lied close to the 2008 Robeson upper bound, reaching up to 25.86 Barrer of CO_2 permeability and a 58.04% increase in selectivity.[171]

Supported ionic liquid membranes (SILMs) represent the most straightforward approach to incorporating ILs into membrane separation technologies, aiming to harness the potential of ILs to create membranes that can efficiently sieve and rapidly transport gas molecules. Nevertheless, the challenge of preventing the leaching of free ILs poses a significant limitation to their effectiveness. Poly(IL)-IL composite membranes are emerging as materials to address this limitation. Their high mechanical stability, derived from strong ionic interactions between the poly(IL) and IL components, result in high CO_2 selectivity, thermal stability and tunable properties, and thus have shown promise for CO_2 separation in gas streams. Yu et al. reported a one-pot method to prepare a tough double network ion gel membranes by a ring opening reaction and free radical polymerization with heating and UV light irradiation.[172] It is found that by increasing the free ILs content in the double network ion gel membrane, the crystallinity and glass transformation temperature of the membrane decreases, resulting in enhanced CO_2 permeability and selectivity. In another report, Lee and Gurkan investigated the CO_2 separation from air with a PIL-IL/GO TFC type of FTM on poly(ethersulfone)/poly(ethylene terephthalate) (PES/PET) substrate (**Figure 11**).[173] The IL, [EMIM][2-CNpyr], acted as the mobile carrier in the poly(IL) fixed carrier, and this incorporation enhanced the CO_2 solubility within the FTM as well as increasing the CO_2-complex mobility. The obtained PIL-IL/GO FTM maintained stability over a continuous separation period of 2 weeks, exhibiting high CO_2 permeance of 3092 GPU at 295 K and 40% RH, with record-breaking CO_2/N_2 selectivity of 1189. The findings indicate that the developed PIL-IL/GO FTM can be potentially integrated into DAC technologies. **Table 3** outlines transport properties of the reviewed polymeric membranes in this section, with some additional selected ones in the last 5 years.

3. Alternative Synthesis Pathways of Polymeric Materials for CO_2 Capture

3.1. Utilization of Bio-Based Materials

Many researchers, in an effort to reduce environmental footprint of polymer production, are exploring bio-based materials for CO_2 capture. Nanocellulose is a sustainable and promising bio-based nanomaterial due to its outstanding mechanical properties, biocompatibility, and natural abundance.[9] Recently, there has been a significant increase in interest regarding the use of nanocellulose, especially as nanofillers in membrane fabrication.

Table 3. Transport properties of selected polymeric membranes.

Strategy	Material	$p(CO_2)$[a] [bar]	T [°C]	$P(CO_2)$ [Barrer]	α (CO_2/N_2)	α (CO_2/CH_4)	Refs.
PEO-based (crosslinking)	BP-70	15	35	1711	44	–	[164]
PEO-based (crosslinking)	PDMS-*b*-PEO	3	30	1768[b]	43.8	–	[165]
	Pebax/PDMS-*b*-PEO/PAN	3	30	2142[b]	36		
PEO-based (crosslinking)	PEO/PDMS(20)	3.5	25	423	43	–	[174]
	PEO/PDMS(20)	3.5	35	528	35		
	PEO/PDMS(20)	3.5	50	888	25		
	PEO/PDMS-PDMS(UV)-PAN	3.5	35	2650[b]	20		
PEO-based	XLPEO	3.0	30	223	47	–	[175]
(imine-linked/N-doped)	N-POPs/XLPEO	3.0	30	420.2	55.3		
	N-CSs/XLPEO	3.0	30	540.4	61.3		
Pebax/PDMS/PSf (air plasma	AP-10-$0.25_{0.5}$	1	25	2022[b]	~30.0	–	[176]
assisted spray coating)	AP-10-$0.25_{0.5}$	10	25	752[b]	13.3		
Perfluoropolymer	Cytop	9	35	25.2±1.5	–	27±3	[177]
	Poly(50%PBVE-*co*-50%PDD)	9	35	228±18		16±2	
PI-based (MOFs	M-0	10	35	6.2	–34.1	31	[170]
incorporation)	M-0	10	30	7.24	37.56	36.2	
	M-10	10	30	11.56	42	38.9	
	M-20	10	30	15.10	48.45	46	
	M-30	10	30	20.54		54.67	
PI-based (MOFs	MMM-10%MOF	10	25	13.2	–	41.58	[171]
incorporation)	MMM-20%MOF	10	25	18.34		46	
	MMM-30%MOF	10	25	25.86		57.21	
PI-based (MOFs	PI	1	35	6.86	–	29.82	[178]
incorporation)	PI-ZnBDC-0.75	1	35	9.17		28.66	
	PI-ZnO@ZnBDC-0.5	1	35	10.08		36.00	
	PI-ZnO@ZnBDC-0.75	1	35	11.46		39.52	
	PI-ZnO@ZnBDC-1	1	35	9.79		31.58	
	PI-ZnO@ZnBDC-1.5	1	35	8.17		28.17	
Poly(IL) (double network)	DNPoly[VEIM][TFSI]:[EMIM][TFSI](80%)	1	35	866	31	–	[172]
	DNPoly[VEIM][TFSI]:[EMIM][DCA](70%)	1	35	464	63		
Poly(IL)/GO FTM	PIL-IL/GO on PES/PET substrate	1	22	3092[b]	1189	–	[173]
Poly(IL) FTM	Poly([Veim][Gly])	0.01	30	≈1400[b]	>2000	–	[179]
Copoly(IL)	M1(IL1-*co*-AM)	2	[c]	52[b]	66	–	[180]
	M2(IL1-*co*-3AM)	2	[c]	76[b]	53		
Pebax/PEG ion gel membrane	Pebax 1657/tetra-PEG IPN/[Emim][C(CN)$_3$]	1	80	≈3100	43	–	[181]

[a] $p(CO_2)$ = CO_2 partial pressure, 1 atm = 101.325 kPa; $P(CO_2)$ = CO_2 permeability; α = ideal CO_2/gas selectivity; [b] Permeance measured in hollow fiber or TFC membrane, GPU; [c] Not stated.

Janakiram and co-workers[182] reported on the functionalization of nanocellulose fibers in sterically hindered polyallylamine (SHPAA)/PVA blend FTMs. Incorporating functionalized nanocellulose into the SHPAA/PVA blend FTMs resulted in improved CO_2 permeability up to 652 GPU and high CO_2/N_2 separation of 41.3 compared to neat PVA membranes. Dai et al. discovered that different types of nanocellulose may result in different interactions and dispersion patterns within the polymer matrix, leading to different variations of CO_2 capture performances.[183] In their work, nanocellulose crystals (CNCs) and nanocellulose fibers (CNFs) were incorporated into poly(vinyl alcohol) (PVA) and applied as selective layers on hollow-fiber membrane substrates through dip-coating to enhance CO_2 capture. The CNCs demonstrated greater improvement in CO_2 permeance and CO_2/N_2 selectivity than CNFs, with a value of 672 GPU and 43.6, respectively. Additionally, the CNC modified membrane exhibited outstanding long-term stability, maintaining its performance for up to a year.

Another biopolymer that is promising as a membrane material for CO_2 capture is chitosan. While this semicrystalline and water-swelling biopolymer contains abundant amine groups that support CO_2 molecule transport, it does have solubility limitations and is, only soluble in aqueous solution with a pH value below 6.5. Therefore, chitosan is often modified as carboxymethyl chitosan (CMC), a natural polyelectrolyte, that has good solubility in alkaline solutions. In alkaline solutions, CMC acquires an overall negative charge, while the carboxyl groups can serve as the carriers in the FTMs.[184] Li et al. utilized CMC, piperazine, and trimesoyl chloride to prepare TFC membranes with

different Turing nanostructures via interfacial polymerization on the polydimethylsiloxane (PDMS)/PSf support.[185] Interestingly, by altering the loading of CMC, the morphology of the membrane surface changed from corrugated nanostructures in the absence of CMC, to well-organized networks, such as octopus-branched structures and nodular structures at high CMC loading. The differing strengths of intermolecular hydrogen bonds was mentioned as the reason why these various Turing nanostructures were observed. In addition to changing surface morphology, adding CMC to the TFC membranes also enhanced CO_2 permselectivity, showing optimal CO_2 permeance of 1278 GPU and CO_2/N_2 selectivity of 89 at 1.5 bar for the octopus-branched membrane. Chitosan nanofibers have been used as a MOF nanofibrous membrane template by Jiamjiranngkul et al.[186] In their work, Cu-BTC-incorporated chitosan/PVA nanofibrous membrane (Cu-BTC/CNFs) hybrids were successfully synthesized by sequentially depositing Cu^{2+} as a metal cluster and BTC as an organic precursor to generate Cu-BTC MOF particles on the surface of the nanofibers through a layer-by-layer approach. The CNFs/Cu/BTC-3 composite had micropores ranging from 0.6 to 0.8 nm, alongside an ≈11-fold increase in specific surface area and the adsorption capacity for CO_2/N_2 over 14 times compared to the neat CNFs.

Amino acids are also being explored for CO_2 capture, due to their amine groups for CO_2 transport beneficiation. Zhang et al. reported the utilization of amino acid salts as mobile carriers in FTMs with PVAm as the FSC.[187] The alanine (Ala), lysine (Lys), and proline (Pro) salts were prepared by deprotonation with 2-(1-piperazinyl)ethylamine (PZEA). The study showed that the obtained FTMs exhibited good thermal stability, and the order of effectiveness to facilitate CO_2 transport was PZEA-Pro>PZEA-Lys>PZEA-Ala with a promising CO_2 permeance of 936 GPU and CO_2/N_2 selectivity of 210, surpassing the Robeson and modified upper bound. In correlation to these findings, Chen and coworkers investigated the amine-CO_2 reaction chemistry of several multiamine amino acid salts by ^{13}C NMR spectroscopy.[188] It was found that amino acid salts with higher steric hindrance demonstrated a higher CO_2 loading as well as higher CO_2 permeances of FTMs for postcombustion CO_2 capture.

3.2. Reversible Addition-Fragmentation Chain Transfer (RAFT) Polymerization

One of the main challenges in well-defined polymer synthesis is control of the molecular weight with low dispersity ($Đ$). Among many reversible deactivation radical polymerization (RDRP) processes, a versatile method to synthesize a variety of functional polymers with controlled composition, controlled molecular weight, and very low dispersity (usually $Đ < 1.2$; sometimes $Đ < 1.1$) is the RAFT polymerization.[189,190] RAFT polymerization was invented by Rizzardo, Moad, and Thang in 1998.[190] The process is mediated by a RAFT agent (thiocarbonylthio compound, S = C(Z)S-R) to control the radical polymerization.[190] The mechanism involves a reversible addition-fragmentation sequence, in which the living character of the polymerization conferred by the transfer of the S = C(Z)S- moiety between active and dormant chains. The choice of Z and R in the thiocarbonylthio compound is crucial to a successful RAFT polymerization. The Z group should activate the C=S double bond toward radical addition, while the R group should be a good radical homolytic leaving group, and as an expelled radical (R•), should effectively reinitiate radical polymerization.[191] Numerous thiocarbonylthio RAFT agents that includes aromatic and aliphatic dithioesters, trithiocarbonates, dithiocarbamates, and xanthates, for various monomers polymerizations have now been reported and successfully used in the RAFT polymerization.[192–195]

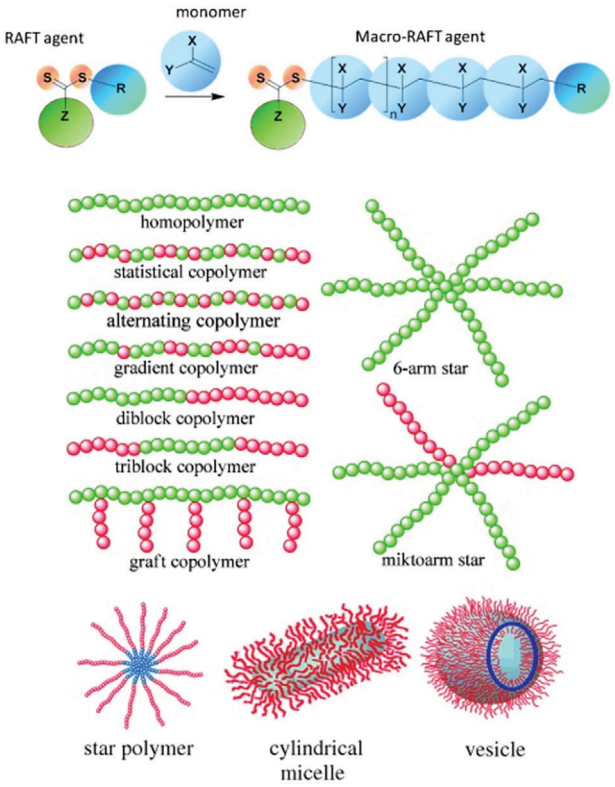

Figure 12. The overall process and accessible polymer architectures by RAFT polymerization. Reproduced with permission.[196] Copyright 2013, John Wiley and Sons.

Above and beyond its livingness, the RAFT process is also known for its compatibility with a broad range of monomers, effectively carried out over a wide range of reaction conditions, tolerant of various functional groups, and free of metal catalyst. It provides a route to the synthesis of polymers containing end or side chain functionality by a one-step process without the need for protection or deprotection strategies, this understandably is an advantage in the synthesis of block copolymers and other more complex architecture polymers.[193,196] Hard-soft, hydrophilic–hydrophobic,[194] and other block copolymers containing various functionality[195] have been reported, which can be carried out in bulk, solution, emulsion, or suspension using standard conditions.[197] Star polymers has also been successfully synthesized via RAFT polymerization,[198] indicating its wide applicability in designing polymers for different applications. The overall process and accessible polymer architectures by RAFT polymerization are displayed in **Figure 12**.

In terms of CO_2 capture, the RAFT method allows the fine-tuning of polymer architecture and the inclusion of various

functional groups to design CO_2-responsive materials. To date, the synthesis of a range of precise polymer architectures using RAFT have attained CO_2-responsive properties and are being developed further for incorporation in CO_2 capture technologies. These includes diblock,[199] and triblock copolymers,[200] graft copolymers,[201] and even the more complex star polymers.[202] Guo et al., for example, utilized hydrophilic units of PEG, CO_2-sensitive monomer of *N,N*-diethylaminoethyl methacrylate (DEAEMA), and the hydrophobic monomer of benzyl methacrylate (BzMA) to synthesize a variety of well-defined statistical, block, and gradient copolymers.[203] By employing both batch and semibatch RAFT polymerization techniques, this process resulted in CO_2-responsive nano-objects that self-assembled with bubbling CO_2 to nanosheet-like structures for the gradient copolymers and large vesicles with thinner membrane thickness for the block and statistical copolymers. Moreover, Guo and co-workers reported a facile synthesis for producing well-defined CO_2-responsive gradient copolymers, denoted as PBzMA-*b*-P(DEAEMA-*grad*-NVP)-*b*-PNVP, using switchable RAFT polymerization.[204] These amphiphilic gradient copolymers exhibit controlled self-assembly into various multicompartment micelles in the presence of specific solvents. The micelles feature patchy, noncontinuous subdomains that surround the inner micelle cores. The authors suggest that this gradient copolymers strategy holds promise for pioneering precise morphological design and realization. More recently, this group showcased a dual gas-responsive polymeric vesicle system by assembling amphiphilic triblock copolymers PEO-*b*-P(DEAEMA-*co*-FMA)-*b*-PS, composed of hydrophilic PEO segments, hydrophobic PS segments, and random copolymer segments comprising O_2-responsive poly(2,2,2-trifluoroethyl methacrylate) (PFMA) units along with CO_2-responsive PDEAEMA units.[200] The RAFT-derived triblock copolymers resulted in well-defined structures and very low dispersity (ranging from 1.36 to 1.58). The amphiphilic and gas-responsive segments enable these triblock copolymers to self-assemble in aqueous solutions, transitioning morphologically from nanotubes to vesicles upon gas stimulation. Interestingly, during CO_2/O_2 stimulation cycles, the vesicles can expand and contract in volume, thus driving morphology changes and shape transformations for mimicking the formation, respiration, and apoptosis of the alveoli.[200]

Developing polymers with switchable functionalities is also viable with RAFT. These smart multiresponse polymers undergo reversible phase transitions or changes in response to external stimuli, such as temperature, pressure, or pH, to allow efficient regeneration of materials in CO_2 capture processes. Yin et al. prepared RAFT copolymerization of DEAEAM monomer with *N*-isopropylacrylamide (NIPAM) that resulted in the production of either statistical or diblock copolymers with dual thermo- and CO_2-responsiveness behavior.[205] Their method offers the flexibility to adjust the cloud point (CP) temperature by altering the composition or architecture (statistical, block) or through CO_2 addition/removal. Likewise, the RAFT synthesis of a series of thermo-, pH-, and CO_2- triple-responsive homopolymers containing ethoxy groups and terminated with pyrrolidine, piperidine, *N*-methylpiperazine, morpholine, and thiomorpholine end substituents, was reported by Wang et al.[206] Upon exposure to CO_2, all polymers exhibited complete solubility, with their lower critical temperature (LCST) behavior recovering by the introduction of N_2, even though there was a discrepancy observed with the initial CP. Their findings reveal the significant influence of various heterocyclic substituents on polymer responsiveness, offering valuable insights into the stimulation response properties of polymers and suggesting pathways for the design of novel CO_2-responsive polymers. Furthermore, Wang and co-workers presented a study on RAFT polymerization of homopolymers containing hydrophilic ethoxy group, amino group, and ferrocene (Fc), with quadruple-responsiveness properties.[207] The obtained homopolymers displayed four different stimuli responses, i.e., temperature, pH, CO_2, and redox. Specifically, the CO_2 responsiveness was verified by cyclic bubbling of CO_2/N_2 through the solution. These homopolymers exhibit amphiphilic properties and self-assembly behavior in solution. Results indicate that they have various critical micelle concentrations and the ability to form lamellar, spherical, and agglomerated structures, in which the morphologies can undergo reversible changes under applied stimulation.

In the last 5 years, the RAFT method has also contributed in the design of adsorbent materials and membranes for CO_2 capture. Haridharan et al. successfully synthesized phyllosilicate-anchored poly(quaternary-ammoniumhydroxidemethyl styrene) nanocomposites to enhance CO_2 adsorption.[208] The nanocomposite was effectively synthesized using the high reactivity of trithiocarbonate macrochain transfer agent (macro-CTA) facilitated by RAFT polymerization, in which the macro-CTA was essential for controlling molecular weight growth from the phyllosilicate surface and preserving living chains with lower dispersity values. The resulting phyllosilicate/polymer nanocomposites exhibited CO_2 uptake of up to 2 mmol g^{-1} at 25 °C. Tiainen and co-workers reported the preparation of poly(aminoethyl methacrylate) (PAEMA), poly-(ethylene oxide)-*block*-(aminoethyl methacrylate) (PEO-*b*-PAEMA), and their guanidinylated derivates, namely PGEMA and PEO-PGEMA, via RAFT polymerization to study their CO_2 adsorption properties.[209] It was found that these polymers exhibit high CO_2 capacity, with the highest value of 2.4 mmol g^{-1} at room temperature, achieved by PGEMA with 7% guanidinylation degree. Low desorption temperature was also observed, thus requiring low energy for regeneration.

Politakos and co-workers reported the CO_2 adsorption performances of reduced GO (rGO) monolithic materials incorporated by CeO_2 particles which were grafted with functionalized polymer brushes by RAFT polymerization.[210] Polymer brushes of poly(acrylic acid) (PAA), poly(vinyl caprolactam) (PVCL), and poly [(2-methacryloyloxy)ethyl) trimethylammonium chloride] (PMETAC) were grafted from the surface of the CeO_2 particles. The result shows that the rGO/CeO_2/PVCL exhibited the highest CO_2 adsorption of 0.64 mmol g^{-1}, whereas the lowest value (of 0.5 mmol g^{-1}) was obtained by the rGO/CeO_2/PMETAC. Findings indicate that the presence of various functionalities (for example different chemical groups) significantly influenced the CO_2 adsorption, while specific surface areas and total pore volumes exert a minimal impact. Additionally, the acidity of the CO_2 played a role in the adsorption process, potentially affecting the conformation of particles coated with polymer brushes, which might undergo structural changes under acidic gas conditions. In another report, RAFT-derived imidazolium-based homo- and copoly(IL)s followed by anion metathesis reactions were

successfully prepared by Nellepolli and co-workers.[211] The synthesized poly(vinylimidazolium)-*co*-polystyrene copolymers exhibited high thermal stabilities up to 300 °C, rendering them suitable for post-combustion CO_2 separation. The copolymers were unable to form free-standing membranes due to their brittle nature, thus blending with commercially available [C_2mim][NTf_2] IL was performed. These membranes exhibited CO_2 permeabilities ranging from 16.5 to 24.5 and CO_2/N_2 permselectivities from 31.7 to 34.4.

3.3. Computational Modeling and Design

Developing a predictive model for forecasting CO_2 capacity is essential. Nowadays, the attempts to predict materials early that will exhibit enhanced CO_2 capture performances, particularly polymer structures, and then optimize their performance, has become more viable thanks to the rapid development of computational studies. Artificial Neural Networks (ANNs) is one of the mathematical models that is beneficial for modeling processes that lack clear physical or chemical descriptions. Moradi and coworkers used ANN and response surface methodology to investigate the influence of independent variables, such as synthesis time, ratio of crosslinker, duration of adsorption, pressure, and temperature, toward adsorption capacity.[212] Torkashvand et al. developed carbazole-based HCPs and then their adsorption process was investigated based on the ANN and response surface methodology model.[117] The optimum value of adsorption capacity at 174.59 mg g^{-1} was achieved, as well as the effects of adsorption time, ratio of crosslinker, duration of synthesis, and their interactions on the quantity of CO_2 adsorbed were also examined.

Aksu et al. performed a computational screening strategy based on structure to identify the most suitable hypothetical COF (hypoCOF) adsorbents and membranes for CO_2 capture and H_2 purification.[213] Two hypoCOF subsets were constructed, namely hypoCOF-A set for adsorbents and hypoCOF-M set for membranes, by filtering the materials based on their largest cavity diameter (LCD) and porosity values. Several chemical descriptors, such as dimensionality, linker and bond types, and topological nets were examined. By Grand Canonical Monte Carlo (GCMC) simulations using the RASPA software (version 2.0.36), the CO_2/H_2 separation efficiency of hypoCOF-A set, with a large number of 3184 hypoCOFs, was assessed for both pressure-swing adsorption (PSA) and vacuum-swing adsorption (VSA) processes. Density functional theory (DFT) calculations were employed to understand the effect of linker types on CO_2 and H_2 adsorption of the two hypoCOF subsets. The findings indicated that CO_2 and H_2 form van der Waals interaction with the linkers and the hydrogen bonding strength between CO_2 and linker functional groups plays a crucial role in the CO_2 selectivity of hypoCOFs. Linkers having —OH functional groups are among the top hypoCOFs exhibiting high CO_2/H_2 adsorption selectivity (S_{ads}), due to their stronger hydrogen bond with CO_2, that increases CO_2 affinity. Meanwhile, molecular dynamics (MD) simulations on 794 hypoCOFs in the hypoCOF-M set demonstrated that they surpass the Robeson upper limit, due to their enhanced H_2 permeabilities (9×10^5–4.5×10^6 Barrer) and higher H_2/CO_2 selectivities (2.66–6.14) compared to polymeric membranes. This research offers molecular-level guidance for the development of new materials with enhanced CO_2 separation capabilities by highlighting key structural attributes of hypoCOFs. Most recently, Zhang et al. employed GCMC and DFT to investigate the adsorption and separation capabilities of CO_2, N_2, and CH_4 within 2D COFs stabilized by alkali metals, such as Li, Na, and K.[214] In order to uncover the fundamental mechanism behind the ultrahigh enhancement of CO_2 capture and separation performances through anchoring Li/Na/K, various factors were also examined, including structural stability, pore characteristics, isothermal adsorption heat, van der Waals and Coulomb forces, gas distribution density, adsorption configurations, and the gas radial distribution function. Machine learning (ML) algorithms, Monte Carlo simulations, and DFT calculations are also reported to be employed in studies of IL optimal loading in IL/COF composites for CO_2/N_2 separations.[215]

In the construction of FTMs, computational methods can be employed to provide insights of the design and selection of carrier structures to achieve better separation efficiency. These computational methods are also very useful for researchers in validating their experimental data. Deng and co-workers utilized a series of theoretical approaches to investigate FTM systems.[216] They used DFT to explore the amine–CO_2 interactions within poly(N-vinylformamide-*co*-vinylamine) (PNVF-*co*-VAm) fixed-site with PZ-Gly and PZEA-Sar as mobile carriers. Moreover, molecular dynamics (MD) simulations via Monte Carlo methods was employed for examining the mobility of carriers and diffusivities of guest molecules, such as CO_2, N_2, and water, as well as the solubility of N_2. This marked the first comprehensive molecular-level analysis of mobile carriers in the FTM system, in which the computational findings were aligned to the experimental data. The insights obtained are expected to accelerate the search for identifying potential mobile carrier candidates.

Utilizing computational modeling and theoretical algorithms can be more cost-effective and time-efficient than laboratory experiments. It also allows simulations scaling up real industrial application conditions. Meng and co-workers developed a mathematical model to explore single-stage membrane gas separation for precombustion, focusing on how the performance of CO_2 capture is influenced by membrane properties (permeability and selectivity) and operational parameters like feed and permeate pressures, along with the feed flow rate.[217] The findings from the simulations successfully identified the optimal conditions essential for an efficient CO_2 capture process using actual industrial syngas and underscore the effectiveness of FTMs in CO_2 removal within both oxygen-blown and air-blown integrated coal gasification combined cycle (IGCC) processes.

4. Conclusion and Future Outlook

In this review, we have presented the most recent advances of polymeric materials in the domain of CO_2 capture. Intelligent design of modern amine-based polymers, POPs, and polymeric membranes that exhibit promising absorption or adsorption capabilities, alongside with competitive separation and permeation features are showcased. Innovative synthesis pathways, including bio-based materials, the advantage of RAFT polymerization, and employing computational modeling provides new insights for researchers to creatively design advanced polymer-based

materials. Nonetheless, it is clear that the endeavor of CO_2 capture using polymer-based materials is still emerging, with significant advancements in material design and processes required urgently to address the fast-paced global climate change. The final remarks and future outlook are summarized as follows:

1) Amine-based polymers are most widely used in CO_2 capture due the rich amine-CO_2 interaction. PEI is noted for its dense amine groups and are commonly added to solid supports by employing techniques such as impregnation, grafting, and copolymerization to improve adsorption. PVAm is prominent especially within FTMs for its effective CO_2 transport and chemisorption capabilities. The PVAm FTMs itself have seen significant development, from pre-pilot implementations in coal-fired plants to pilot-scale applications with high CO_2 purity levels. Moreover, the innovative use of PAN in CO_2 capture technology, highlights its roles in nanofiber adsorbents, membrane separation, and hybrid material development. PAN nanofibers, are known for their high surface area and efficiency which can be further improved through methods like electrospinning, doping, and temperature optimization. Despite their cost-effectiveness, simple synthesis, and CO_2 selectivity, these amine-based polymers are susceptible to oxidative and mechanical degradation. Future designs mostly will continue using innovations that integrate protective additives to ensure durability and efficiency in CO_2 capture processes, such as MOFs and nanoparticles, aiming at efficient, stable, and scalable CO_2 capture solutions.
2) POPs provide low density, extensive surface areas, customizable pore sizes, and ample active sites for chemical reactions. This category of polymer includes amorphous CMPs that are synthesized by coupling reactions like Sonogashira–Hagihara reaction and Suzuki–Miyaura reaction, HCPs through Friedel–Crafts alkylation, and crystalline COFs that are structured frameworks made from organic building blocks connected through covalent bonds. They stand out for their low energy regeneration requirements, high stability, and selective CO_2 gas adsorption properties. Moreover, their integration into membrane separation technologies, such as MMCMs and TFC membranes, has demonstrated enhanced CO_2 separation performance. Recent approaches for developing these materials involve chemical modifications to maximize surface area and porosity, adding polar units for more adsorption sites, postsynthetic functionalization, and the integration of ILs. Many POPs are synthesized using costly monomers and removal of their residual metal catalysts are challenging, thus future developments should explore more on simple synthetic routes using sustainable materials and metal-free methods with life-cycle assessments for reduced environmental impact. POPs stand as a progressive field in materials science and further advocating for its wider adoption in industrial production is essential.
3) Polymeric membranes are especially valued for their selectivity, energy efficiency, less corrosive, and minimal byproducts, despite facing challenges like the permeability-selectivity trade-off. To surpass these limitations, research is directed toward developing new polymeric membranes that are primarily aimed at enhancing performance and to mitigate issues such as high crystallinity in membranes. The current strategies include the use of block copolymers, TR polymers, perfluoropolymers, and FTMs, while advanced innovations by the incorporation of MOFs as nanofillers or developing SILMs, highlight the ongoing efforts to improve CO_2 separation efficiency. For industrial applications, it is important to overcome its high manufacturing cost and that membrane materials are assessed in real-world and challenging separation scenarios, which includes their degradation/fouling challenges.
4) Several alternative synthesis pathways have been outlined to develop advanced polymer-based materials for CO_2 capture. The role of bio-based materials, in particular nanocellulose, chitosan, and amino acids, offers efficient and sustainable solutions to environmental challenges. RAFT polymerization has led to the development of CO_2-responsive polymers capable of forming CO_2-responsive nanostructures and producing advanced adsorbent materials and membranes with improved CO_2 adsorption properties. Through innovations like polymeric nanocomposites and functionalized polymer brushes, RAFT polymerization offers a flexible and efficient strategy for developing precise polymer materials, showing great promise in enhancing CO_2 capture and separation technologies. Moreover, machine learning algorithms and theoretical approaches can be further applied to assess the design and CO_2 performance of polymer materials. Advancements in computational studies will continue on to improve the feasibility and optimization of polymer materials, offering valuable insights for the rapid development of new polymeric materials and technologies for CO_2 capture and separation in industrial settings.
5) The future of developing polymer-based materials in direct air capture (DAC) of CO_2 is promising and evolving, as recently studied PEI-, PAN-, COFs-based porous adsorbents, and polymeric FTMs have demonstrated high selectivity of CO_2 capture at low concentrations (<400 ppm) and relevant for direct air capture (DAC) applications. Ongoing research will be focusing on enhancing material CO_2 adsorption efficiency and selectivity, faster capture and release kinetics, as well as the durability and stability, as they must withstand numerous adsorption–desorption cycles without losing effectiveness, even under extreme environmental factors such as humidity. Additionally, reducing the energy required for material regeneration presents a significant challenge, thus advances in polymer chemistry should develop materials that regenerate with less energy, alongside with the synergistic integration of DAC developments with renewable energy sources and existing CCUS technologies.

Finally, despite the significant gap between laboratory research and industrial application, the advent of novel polymeric materials and their property improvements are expected to bring more vitality into all CCUS technologies. Polymer-based materials holds promise for CO_2 capture, and more efforts are warranted to promote its industrial deployment to achieve the net-zero target and combat climate change.

Acknowledgements

M.G.D. would like to acknowledge the Australia Awards Scholarship (AAS) for the awarded Ph.D. scholarship and for the financial support provided. S.H.T. acknowledged funding support from the Australian Research Council for the ARC Centre of Excellence for Enabling Eco-Efficient Beneficiation of Minerals (Grant No. CE200100009).

Open access publishing facilitated by Monash University, as part of the Wiley - Monash University agreement via the Council of Australian University Librarians.

Conflict of Interest

The authors declare no conflict of interest.

Keywords

adsorbents, amine-based polymers, CO_2 capture, polymer-based materials, polymeric membranes, porous organic polymers, RAFT polymerization

Received: March 5, 2024
Revised: April 30, 2024
Published online: May 13, 2024

[1] I. Sreedhar, T. Nahar, A. Venugopal, B. Srinivas, *Renewable Sustainable Energy Rev.* **2017**, *76*, 1080.
[2] BritishPetroleum, Statistical Review of World Energy, https://www.bp.com/content/dam/bp/business-sites/en/global/corporate/pdfs/energy-economics/statistical-review/bp-stats-review-2022-full-report.pdf, (accessed: August, 2022).
[3] H. Ritchie, M. Roser, P. Rosado, CO_2 and Greenhouse Gas Emissions, https://ourworldindata.org/emissions-by-sector, (accessed: August, 2022).
[4] V. Masson-Delmotte, P. Zhai, H.-O. Pörtner, D. C. Roberts, J. Skea, P. R. Shukla, A. Pirani, W. Moufouma-Okia, C. Péan, R. Pidcock, S. Connors, J. B. R. Matthews, Y. Chen, X. Zhou, M. I. Gomis, E. Lonnoy, T. Maycock, M. Tignor, T. Waterfield, Summary for Policy Makers: Global Warming of 1.5° C. An IPCC Special Report on the Impacts of Global Warming of 1.5 °C Above Pre-Industrial Levels and Related Global Greenhouse Gas Emission Pathways, in the Context of Strengthening the Global Response to the Threat of Climate Change, Sustainable Development, and Efforts to Eradicate Poverty, Cambridge, UK, **2018**.
[5] C. Bettenhausen, *Chem. Eng. News* **2021**, *99*, 28.
[6] IEA, *Transforming Industry through CCUS*, IEA, Paris **2019**.
[7] B. Dziejarski, J. Serafin, K. Andersson, R. Krzyżyńska, *Mater. Today Sustainability* **2023**, *24*, 100483.
[8] S. Zhang, Y. Shen, L. Wang, J. Chen, Y. Lu, *Appl. Energy* **2019**, *239*, 876.
[9] N. A. D. Ho, C. P. Leo, *Environ. Res.* **2021**, *197*, 111100.
[10] K. A. Mumford, Y. Wu, K. H. Smith, G. W. Stevens, *Front. Chem. Sci. Eng.* **2015**, *9*, 125.
[11] IPCC, *IPCC Special Report on Carbon Dioxide Capture and Storage*, IPCC, Cambridge **2005**.
[12] A. Sattari, A. Ramazani, H. Aghahosseini, M. K. Aroua, *J. CO2 Util.* **2021**, *48*, 101526.
[13] D. Jansen, M. Gazzani, G. Manzolini, E. van Dijk, M. Carbo, *Int. J. Greenhouse Gas Control* **2015**, *40*, 167.
[14] J. D. Figueroa, T. Fout, S. Plasynski, H. McIlvried, R. D. Srivastava, *Int. J. Greenhouse Gas Control* **2008**, *2*, 9.
[15] E. S. Sanz-Pérez, C. R. Murdock, S. A. Didas, C. W. Jones, *Chem. Rev.* **2016**, *116*, 11840.
[16] A. Sodiq, Y. Abdullatif, B. Aissa, A. Ostovar, N. Nassar, M. El-Naas, A. Amhamed, *Environ. Technol. Innovation* **2023**, *29*, 102991.
[17] M. Ozkan, *MRS Energy Sustainability* **2021**, *8*, 51.
[18] M. Fasihi, O. Efimova, C. Breyer, *J. Cleaner Prod.* **2019**, *224*, 957.
[19] A. Zaker, S. ben Hammouda, J. Sun, X. Wang, X. Li, Z. Chen, *J. Environ. Chem. Eng.* **2023**, *11*, 109741.
[20] B. Petrovic, M. Gorbounov, S. M. Soltani, *Microporous Mesoporous Mater.* **2021**, *312*, 110751.
[21] C. Quan, Y. Zhou, J. Wang, C. Wu, N. Gao, *J. CO2 Util.* **2023**, *68*, 102373.
[22] H. A. Patel, J. Byun, C. T. Yavuz, *ChemSusChem* **2017**, *10*, 1303.
[23] R. Bottoms, *United States Patent 1783901*, **1930**.
[24] L. Zou, Y. Sun, S. Che, X. Yang, X. Wang, M. Bosch, Q. Wang, H. Li, M. Smith, S. Yuan, *Adv. Mater.* **2017**, *29*, 1700229.
[25] G. T. Rochelle, *Science* **2009**, *325*, 1652.
[26] Y. Zhang, B. Freeman, P. Hao, G. T. Rochelle, *Faraday Discuss.* **2016**, *192*, 459.
[27] C. Kim, S. N. Talapaneni, L. Dai, *Mater. Rep.: Energy* **2023**, *3*, 100199.
[28] S. Kumar, R. Srivastava, J. Koh, *J. CO2 Util.* **2020**, *41*, 101251.
[29] M. Younas, M. Rezakazemi, M. Daud, M. B. Wazir, S. Ahmad, N. Ullah, S. Ramakrishna, *Prog. Energy Combust. Sci.* **2020**, *80*, 100849.
[30] S. Zheng, S. Zeng, Y. Li, L. Bai, Y. Bai, X. Zhang, X. Liang, S. Zhang, *AIChE J.* **2022**, *68*, e17500.
[31] Z. Zhang, Y. Zheng, L. Qian, D. Luo, H. Dou, G. Wen, A. Yu, Z. Chen, *Adv. Mater.* **2022**, *34*, 2201547.
[32] S. G. Gizer, O. Polat, M. K. Ram, N. Sahiner, *Int. J. Energy Res.* **2022**, *46*, 16241.
[33] Z. Lei, B. Chen, Y.-M. Koo, D. R. MacFarlane, *Chem. Rev.* **2017**, *117*, 6633.
[34] M. Zunita, R. Hastuti, A. Alamsyah, K. Khoiruddin, I. Wenten, *Sep. Purif. Rev.* **2022**, *51*, 261.
[35] M. Aghaie, N. Rezaei, S. Zendehboudi, *Renewable Sustainable Energy Rev.* **2018**, *96*, 502.
[36] H. Yamada, *Polym. J.* **2021**, *53*, 93.
[37] S.-I. Nakao, K. Yogo, K. Goto, T. Kai, H. Yamada, *Advanced CO_2 Capture Technologies: Absorption, Adsorption, and Membrane Separation Methods*, Springer, Cham, Switzerland, **2019**.
[38] P. V. Danckwerts, *Chem. Eng. Sci.* **1979**, *34*, 443.
[39] D. M. D'Alessandro, B. Smit, J. R. Long, *Angew. Chem., Int. Ed.* **2010**, *49*, 6058.
[40] G. Sartori, D. W. Savage, *Ind. Eng. Chem. Fundam.* **1983**, *22*, 239.
[41] P. V. Kortunov, M. Siskin, M. Paccagnini, H. Thomann, *Energy Fuels* **2016**, *30*, 1223.
[42] P. V. Kortunov, M. Siskin, L. S. Baugh, D. C. Calabro, *Energy Fuels* **2015**, *29*, 5919.
[43] N. Lai, Q. Zhu, D. Qiao, K. Chen, L. Tang, D. Wang, W. He, Y. Chen, T. Yu, *Front. Chem.* **2020**, *8*, 146.
[44] X. Shen, H. Du, R. H. Mullins, R. R. Kommalapati, *Energy Technol.* **2017**, *5*, 822.
[45] S. Satyapal, T. Filburn, J. Trela, J. Strange, *Energy Fuels* **2001**, *15*, 250.
[46] C. Yan, A. Sayari, *Chem. Eng. J.* **2024**, *479*, 147498.
[47] M. Jaffar, A. Rolfe, C. Brandoni, J. Martinez, C. Snape, S. Kaldis, A. Santos, B. Lysiak, A. Lappas, N. Hewitt, Y. Huang, *Carbon Capture Sci. Technol.* **2024**, *10*, 100179.
[48] C. Kim, Y. Ha, M. Choi, *Acc. Chem. Res.* **2023**, *56*, 2887.
[49] C. Choi, R. L. Kadam, S. Gaikwad, K.-S. Hwang, S. Han, *Microporous Mesoporous Mater.* **2020**, *296*, 110006.
[50] X. Jia, P. Yang, Y. Fan, C. Wang, *Sep. Purif. Technol.* **2024**, *328*, 124992.
[51] H. Shi, J. Yang, Z. Ahmad, H. Zhang, J. Chen, *Sep. Purif. Technol.* **2023**, *325*, 124608.
[52] M. Li, Z. Zhu, J. Liu, J. Jin, L. Du, J. Mi, *Ind. Eng. Chem. Res.* **2022**, *62*, 385.

[53] A. Justin, J. Espín, M. J. Pougin, D. Stoian, T. Schertenleib, M. Mensi, I. Kochetygov, A. Ortega-Guerrero, W. L. Queen, *Adv. Funct. Mater.* **2024**, *34*, 2307430.
[54] W. Li, D. Fu, J. Pan, *Energy Fuels* **2023**, *37*, 15879.
[55] W. Choi, J. Park, C. Kim, M. Choi, *Chem. Eng. J.* **2021**, *408*, 127289.
[56] J. Wu, Y. Chen, Y. Xu, S. Chen, H. Lv, Z. Gan, X. Zhu, R. Wang, C.-H. Wang, T. Ge, *Matter* **2024**, *7*, 123.
[57] Y. Miao, Y. Wang, B. Ge, Z. He, X. Zhu, J. Li, S. Liu, L. Yu, *Adv. Sci.* **2023**, *10*, 2207253.
[58] P. Priyadarshini, G. Rim, C. Rosu, M. Song, C. W. Jones, *ACS Environ. Au* **2023**, *3*, 295.
[59] G. N. Short, E. Burentugs, L. Proaño, H. J. Moon, G. Rim, I. Nezam, A. Korde, S. Nair, C. W. Jones, *JACS Au* **2023**, *3*, 62.
[60] C. Wang, S. Okubayashi, *Carbohydr. Polym.* **2019**, *225*, 115248.
[61] M. Liao, S. Long, P. Zou, K.-Y. Zhang, H.-C. Liang, K. Jiang, D. Xie, F.-M. Yang, *Energy Fuels* **2023**, *37*, 15867.
[62] S. Sani, X. Liu, L. Stevens, H. Wang, C. Sun, *Fuel* **2023**, *351*, 128886.
[63] H. Li, S. Zhang, B. Sengupta, H. Li, F. Wang, S. Li, M. Yu, *J. Membr. Sci.* **2022**, *657*, 120617.
[64] M. Zhao, J. Guo, Q. Xin, Y. Zhang, X. Li, X. Ding, L. Zhang, L. Zhao, H. Ye, H. Li, *Sep. Purif. Technol.* **2023**, *324*, 124512.
[65] Y. Yuan, Z. Qiao, J. Xu, J. Wang, S. Zhao, X. Cao, Z. Wang, M. D. Guiver, *J. Membr. Sci.* **2021**, *620*, 118923.
[66] B. Pascual-José, A. Zare, M. Giamberini, J. A. Reina, A. Ribes-Greus, *Macromol. Rapid Commun.* **2024**, *45*, 2300434.
[67] W. Aframehr, B. Molki, R. Bagheri, N. Sarami, *ACS Appl. Polym. Mater.* **2022**, *4*, 3380.
[68] T. J. Kim, B. Li, M. B. Hägg, *J. Polym. Sci., Part B: Polym. Phys.* **2004**, *42*, 4326.
[69] R. Hou, C. Fong, B. D. Freeman, M. R. Hill, Z. Xie, *Sep. Purif. Technol.* **2022**, *300*, 121863.
[70] R. Casadei, D. Venturi, M. Giacinti Baschetti, L. Giorgini, E. Maccaferri, S. Ligi, *Membranes* **2019**, *9*, 119.
[71] C. Ge, M. Sheng, Y. Yuan, F. Shi, Y. Yang, S. Zhao, J. Wang, Z. Wang, *Carbon Capture Sci. Technol.* **2024**, *10*, 100156.
[72] S. Shin, D. K. Yoo, Y.-S. Bae, S. H. Jhung, *Chem. Eng. J.* **2020**, *389*, 123429.
[73] Y. Yuan, Y. Pan, M. Sheng, G. Xing, M. Wang, J. Wang, Z. Wang, *Chin. J. Chem. Eng.* **2022**, *50*, 168.
[74] K. K. Chen, Y. Han, Z. Zhang, W. W. Ho, *J. Membr. Sci.* **2021**, *628*, 119215.
[75] T.-Y. Chen, X. Deng, L.-C. Lin, W. W. Ho, *J. Membr. Sci.* **2022**, *645*, 120195.
[76] R. Casadei, E. Firouznia, M. G. Baschetti, *Membranes* **2021**, *11*, 442.
[77] Y. Wang, L. Li, X. Zhang, J. Li, C. Liu, N. Li, Z. Xie, *J. Membr. Sci.* **2019**, *589*, 117246.
[78] X. Zhang, X. Ren, Y. Wang, J. Li, *Sep. Purif. Technol.* **2022**, *303*, 122195.
[79] Y. Wang, J. Wang, X. Zhang, J. Li, L. Li, *Sep. Purif. Technol.* **2021**, *270*, 118800.
[80] A. Abbasi, M. M. Nasef, S. Kheawhom, R. Faridi-Majidi, M. Takeshi, E. Abouzari-Lotf, T. Choong, *Radiat. Phys. Chem.* **2019**, *156*, 58.
[81] J. Park, A. Kretzschmar, V. Selmert, O. Camara, H. Kungl, H. Tempel, S. Basak, R. d. A. Eichel, *ACS Appl. Mater. Interfaces* **2021**, *13*, 46665.
[82] J. Zhang, Q. Zhao, S. Wang, X. Tan, *Sep. Purif. Technol.* **2022**, *287*, 120562.
[83] J. Zhang, S. Guo, S. Wang, X. Tan, *Sep. Purif. Technol.* **2023**, *324*, 124635.
[84] A. A. Tourzani, F. Hormozi, M. Asadollahzadeh, R. Torkaman, *Sci. Rep.* **2023**, *13*, 6173.
[85] Z. Imanian, F. Hormozi, M. Torab-Mostaedi, M. Asadollahzadeh, *Sep. Purif. Technol.* **2022**, *289*, 120749.
[86] T. M. Ting, M. M. Nasef, P. Sithambaranathan, *J. Radioanal. Nucl. Chem.* **2017**, *311*, 843.
[87] C. A. Trickett, A. Helal, B. A. Al-Maythalony, Z. H. Yamani, K. E. Cordova, O. M. Yaghi, *Nat. Rev. Mater.* **2017**, *2*.
[88] R. Gaikwad, S. Gaikwad, Y. Kim, S. Han, *Microporous Mesoporous Mater.* **2021**, *323*, 111233.
[89] R. Gaikwad, S. Gaikwad, S. Han, *J. Environ. Chem. Eng.* **2023**, *11*, 111592.
[90] Z. Li, Z. Cao, C. Grande, W. Zhang, Y. Dou, X. Li, J. Fu, N. Shezad, F. Akhtar, A. Kaiser, *RSC Adv.* **2022**, *12*, 664.
[91] S. K. Gebremariam, A. M. Varghese, K. S. K. Reddy, Y. F. AlWahedi, L. F. Dumée, G. N. Karanikolos, *Chem. Eng. J.* **2023**, *473*, 145286.
[92] X. Liu, Q. Zhang, H. Zhu, S. Zhu, *Macromol. Mater. Eng.* **2023**, *308*, 2300173.
[93] Y. Jung, Y. G. Ko, I. W. Nah, U. S. Choi, *Chem. Eng. J.* **2022**, *427*, 131781.
[94] N. Ali, A. A. Babar, Y. Zhang, N. Iqbal, X. Wang, J. Yu, B. Ding, *J. Colloid Interface Sci.* **2020**, *560*, 379.
[95] N. Ali, A. A. Babar, X. Wang, J. Yu, B. Ding, *Adv. Eng. Mater.* **2023**, *25*, 2201335.
[96] K. D. Kersey, G. A. Lee, J. H. Xu, M. K. Kidder, A. H. A. Park, Y. L. Joo, *Adv. Funct. Mater.* **2023**, *33*, 2301649.
[97] H. Han, J. M. Scofield, P. A. Gurr, P. A. Webley, G. G. Qiao, *Chem. Eng. J.* **2023**, *462*, 142087.
[98] O. Selyanchyn, R. Selyanchyn, S. Fujikawa, *ACS Appl. Mater. Interfaces* **2020**, *12*, 33196.
[99] A. Sabetghadam, X. Liu, S. Gottmer, L. Chu, J. Gascon, F. Kapteijn, *J. Membr. Sci.* **2019**, *570*, 226.
[100] T. Sun, W. Zheng, J. Chen, Y. Dai, X. Li, X. Ruan, X. Yan, G. He, *J. Membr. Sci.* **2021**, *639*, 119749.
[101] W. Zheng, Z. Li, T. Sun, X. Ruan, Y. Dai, X. Li, C. Zhang, G. He, *J. Membr. Sci.* **2022**, *650*, 120330.
[102] J.-S. M. Lee, A. I. Cooper, *Chem. Rev.* **2020**, *120*, 2171.
[103] J.-X. Jiang, F. Su, A. Trewin, C. D. Wood, H. Niu, J. T. Jones, Y. Z. Khimyak, A. I. Cooper, *J. Am. Chem. Soc.* **2008**, *130*, 7710.
[104] R. Dawson, D. J. Adams, A. I. Cooper, *Chem. Sci.* **2011**, *2*, 1173.
[105] A. F. Saber, S. U. Sharma, J.-T. Lee, A. F. EL-Mahdy, S.-W. Kuo, *Polymer* **2022**, *254*, 125070.
[106] J. Schmidt, M. Werner, A. Thomas, *Macromolecules* **2009**, *42*, 4426.
[107] Y. Song, P. C. Lan, K. Martin, S. Ma, *Nanoscale Adv.* **2021**, *3*, 4891.
[108] Y. Zhang, C. Zhang, W. Shi, Z. Zhang, Y. Zhao, X. Luo, X. Liu, *New J. Chem.* **2022**, *46*, 6394.
[109] S.-B. Ren, P.-X. Li, A. Stephenson, L. Chen, M. E. Briggs, R. Clowes, A. Alahmed, K.-K. Li, W.-P. Jia, D.-M. Han, *Ind. Eng. Chem. Res.* **2018**, *57*, 9254.
[110] L. Wang, C. Yao, W. Xie, G. Xu, S. Zhang, Y. Xu, *New J. Chem.* **2021**, *45*, 19636.
[111] D. S. Amaraseela, N. M. Sarih, S. Habibu, *Energy Adv.* **2023**, *2*, 1127.
[112] Y. Qiao, N. Lv, X. Xue, T. Zhou, G. Che, G. Xu, F. Wang, Y. Wu, Z. Xu, *ChemistrySelect* **2022**, *7*, 202200234.
[113] C. Yao, D. Cui, Y. Zhu, W. Xie, S. Zhang, G. Xu, Y. Xu, *New J. Chem.* **2019**, *43*, 6838.
[114] V. Guillerm, Ł. J. Weseliński, M. Alkordi, M. I. H. Mohideen, Y. Belmabkhout, A. J. Cairns, M. Eddaoudi, *ChemComm* **2014**, *50*, 1937.
[115] G. Cheng, Y. Han, *New J. Chem.* **2023**, *47*, 21600.
[116] F. Meng, J. Wang, M. Chen, Z. Wang, G. Bai, X. Lan, *ACS Catal.* **2023**, *13*, 12142.
[117] A. Torkashvand, H. Ramezanipour Penchah, A. Ghaemi, *Int. J. Environ. Sci. Technol.* **2022**, *19*, 8835.
[118] M. R. Moradi, A. Torkashvand, H. Ramezanipour Penchah, A. Ghaemi, *Sci. Rep.* **2023**, *13*, 9214.
[119] A. Liu, C. Mollart, A. Trewin, X. Fan, C. H. Lau, *ChemSusChem* **2023**, *16*, 202300019.
[120] B. Karami, B. Bayat, H. R. Penchah, A. Ghaemi, *Fuel* **2024**, *363*, 130929.

[121] N. Chanchaona, C. H. Lau, *Sep. Purif. Technol.* **2024**, *329*, 125145.
[122] V. Davankov, S. Rogozhin, M. Tsyurupa, *United States Patent US 3729457A*, **1973**.
[123] A. Torkashvand, M. R. Moradi, A. Ghaemi, *Case Stud. Chem. Environ. Eng.* **2023**, *8*, 100472.
[124] D. Teng, P. Jin, S. Yang, W. Guo, Z. Zhao, G. Zhou, P. Li, Y. Cao, *Ind. Eng. Chem. Res.* **2023**, *62*, 8602.
[125] X. Liao, B. Pei, R. Ma, L. Kong, X. Gao, J. He, X. Luo, J. Lin, *Catalysts* **2022**, *12*, 62.
[126] W. Xu, M. Chen, Y. Yang, K. Chen, Y. Li, Z. Zhang, R. Luo, *ChemCatChem* **2023**, *15*, 202201441.
[127] L. Shao, N. Liu, L. Wang, Y. Sang, P. Zhan, L. Zhang, J. Huang, J. Chen, *Chemosphere* **2022**, *288*, 132499.
[128] C. Guo, G. Chen, N. Wang, S. Wang, Y. Gao, J. Dong, Q. Lu, F. Gao, *Sep. Purif. Technol.* **2023**, *312*, 123375.
[129] F. Maleki, A. Ghaemi, G. Mir Mohamad Sadeghi, *Environ. Prog. Sustainable Energy* **2023**, *42*, e13954.
[130] Y. Li, J. Zhang, K. Zuo, Z. Li, Y. Wang, H. Hu, C. Zeng, H. Xu, B. Wang, Y. Gao, *Catalysts* **2021**, *11*, 1133.
[131] N. Bagherian, A. R. Karimi, A. Amini, *Colloids Surf. A: Physicochem. Eng. Asp.* **2021**, *613*, 126078.
[132] A. Modak, S. Jana, *Microporous Mesoporous Mater.* **2019**, *276*, 107.
[133] Y. Zeng, R. Zou, Y. Zhao, *Adv. Mater.* **2016**, *28*, 2855.
[134] A. P. Cote, A. I. Benin, N. W. Ockwig, M. O'Keeffe, A. J. Matzger, O. M. Yaghi, *Science* **2005**, *310*, 1166.
[135] C. Kang, Z. Zhang, S. Xi, H. Li, A. K. Usadi, D. C. Calabro, L. S. Baugh, Y. Wang, D. Zhao, *Proc. Natl. Acad. Sci. USA.* **2023**, *120*, e2217081120.
[136] L. Liao, M. Li, Y. Yin, J. Chen, Q. Zhong, R. Du, S. Liu, Y. He, W. Fu, F. Zeng, *ACS Omega* **2023**, *8*, 4527.
[137] Y. Kumar, I. Ahmad, A. Rawat, R. K. Pandey, P. Mohanty, R. Pandey, *ACS Appl. Mater. Interfaces* **2024**, *16*, 11605.
[138] J. Zhao, X. Shen, Y.-F. Liu, R.-Y. Zou, *Langmuir* **2023**, *39*, 16367.
[139] Y. Cheng, L. Zhai, Y. Ying, Y. Wang, G. Liu, J. Dong, D. Z. Ng, S. A. Khan, D. Zhao, *J. Mater. Chem. A* **2019**, *7*, 4549.
[140] P. Guan, J. Qiu, Y. Zhao, H. Wang, Z. Li, Y. Shi, J. Wang, *ChemComm* **2019**, *55*, 12459.
[141] C. Ji, K. Su, W. Wang, J. Chang, E.-S. M. El-Sayed, L. Zhang, D. Yuan, *CCS Chem.* **2022**, *4*, 3095.
[142] H. Lyu, H. Li, N. Hanikel, K. Wang, O. M. Yaghi, *J. Am. Chem. Soc.* **2022**, *144*, 12989.
[143] S. Wei, H. Xin, M. Wang, S. Xu, W. Zhai, S. Liu, L. Wang, S. Liu, Z. Wang, X. Lu, *Adv. Theory Simul.* **2022**, *5*, 2200588.
[144] D. Chakraborty, P. Shekhar, H. D. Singh, R. Kushwaha, C. Vinod, R. Vaidhyanathan, *Chem. –Asian J.* **2019**, *14*, 4767.
[145] Y. Wang, C. Kang, Z. Zhang, A. K. Usadi, D. C. Calabro, L. S. Baugh, Y. D. Yuan, D. Zhao, *ACS Sustainable Chem. Eng.* **2021**, *10*, 332.
[146] Y. Zhang, Z. Chen, Q. Liu, J. Wan, *New J. Chem.* **2022**, *46*, 4555.
[147] M. Shan, X. Geng, I. Imaz, A. Broto-Ribas, B. Ortín-Rubio, D. Maspoch, L. Ansaloni, T. A. Peters, A. Tena, M. E. Boerrigter, *J. Membr. Sci.* **2023**, *691*, 122258.
[148] Z. Kang, Y. Peng, Y. Qian, D. Yuan, M. A. Addicoat, T. Heine, Z. Hu, L. Tee, Z. Guo, D. Zhao, *Chem. Mater.* **2016**, *28*, 1277.
[149] H. Xu, W. Feng, M. Sheng, Y. Yuan, B. Wang, J. Wang, Z. Wang, *Chin. J. Chem. Eng.* **2022**, *43*, 152.
[150] Y. Ying, Z. Yang, D. Shi, S. B. Peh, Y. Wang, X. Yu, H. Yang, K. Chai, D. Zhao, *J. Membr. Sci.* **2021**, *632*, 119384.
[151] H. J. Bora, R. Borpatra Gohain, P. Barman, S. Biswas, N. Sen Sarma, A. Kalita, *ACS Omega* **2023**, *8*, 36065.
[152] Q. Chang, H. Guo, Z. Shang, C. Zhang, Y. Zhang, G. Dong, B. Shen, J. Wang, Y. Zhang, *Sep. Purif. Technol.* **2024**, *330*, 125518.
[153] J. Wang, L. Wang, Y. Wang, F. Yang, J. Li, X. Guan, J. Zong, F. Zhou, J. Huang, Y.-N. Liu, *Chem. Eng. J.* **2022**, *438*, 135555.
[154] J. Wang, L. Wang, D. Zhang, Y. Wang, Y. Cao, X. Wang, J. Li, J. Huang, Y.-N. Liu, *Chem. Eng. Sci.* **2023**, *281*, 119171.
[155] Z. Xu, W. Wang, B. Chen, H. Zhou, Q. Yao, X. Shen, Y. Pan, D. Wu, Y. Cao, Z. Shen, *ChemComm* **2023**, *59*, 14435.
[156] M. Yin, L. Wang, S. Tang, *ACS Appl. Mater. Interfaces* **2022**, *14*, 55674.
[157] Y. Han, W. W. Ho, *J. Membr. Sci.* **2021**, *628*, 119244.
[158] A. Basile, A. Iulianelli, F. Gallucci, P. Morrone, in *Developments and Innovation in Carbon Dioxide (CO2) Capture and Storage Technology*, Vol. *1*, (Ed: M. M. Maroto-Valer), Woodhead Publishing, Cambridge, **2010**, p. 203.
[159] C. A. Terraza, L. H. Tagle, J. L. Santiago-García, R. J. Canto-Acosta, M. Aguilar-Vega, R. A. Hauyon, D. Coll, P. Ortiz, G. Perez, L. Herrán, *Polymer* **2018**, *137*, 283.
[160] L. M. Robeson, *J. Membr. Sci.* **1991**, *62*, 165.
[161] L. M. Robeson, *J. Membr. Sci.* **2008**, *320*, 390.
[162] A. Brunetti, F. Scura, G. Barbieri, E. Drioli, *J. Membr. Sci.* **2010**, *359*, 115.
[163] I. Blume, I. Pinnau, *United States Patent US 4963165* **1990**.
[164] W.-S. Sun, M.-J. Yin, W.-H. Zhang, S. Li, N. Wang, Q.-F. An, *Green Energy Environ.* **2023**, *8*, 1389.
[165] J. Liu, Y. Pan, J. Xu, Z. Wang, H. Zhu, G. Liu, J. Zhong, W. Jin, *J. Membr. Sci.* **2023**, *667*, 121183.
[166] J. D. Moon, A. T. Bridge, C. D'Ambra, B. D. Freeman, D. R. Paul, *J. Membr. Sci.* **2019**, *582*, 182.
[167] A. Naderi, A. A. Tashvigh, T.-S. Chung, *J. Membr. Sci.* **2019**, *572*, 343.
[168] F. Cao, H. Gao, Q. Xiong, Z. Liang, *Int. J. Greenhouse Gas Control* **2019**, *82*, 210.
[169] H. Fu, K. Xue, Z. Li, H. Zhang, D. Gao, H. Chen, *Energy* **2023**, *263*, 125677.
[170] S. Bano, S. R. Tariq, T. Anjum, M. Najam, M. Usman, M. Yasin, H. Shafi, A. L. Khan, *Chemosphere* **2022**, *307*, 136051.
[171] A. R. Tariq, S. R. Tariq, M. Sultan, T. Mahmud, G. A. Chotana, *Arabian J. Chem.* **2020**, *13*, 8979.
[172] Y. Yu, X. Yang, C. Zhang, J. Chen, W. Lin, J. Meng, *Sep. Purif. Technol.* **2024**, *331*, 125591.
[173] Y.-Y. Lee, B. Gurkan, *J. Membr. Sci.* **2021**, *638*, 119652.
[174] Y. Chen, M. He, J. Zhang, Y. Su, Z. Xue, C. He, Y. Ji, K. Guan, J. Zhao, H. Matsuyama, *Chem. Eng. J.* **2023**, *478*, 147530.
[175] R. Li, Y. Yang, Z. Zhang, S. Lian, C. Song, *J. Membr. Sci.* **2024**, *690*, 122203.
[176] X. Jiang, K. Goh, R. Wang, *J. Membr. Sci.* **2022**, *658*, 120741.
[177] M. A. El-Okazy, L. Liu, Y. Zhang, S. E. Kentish, *J. Membr. Sci.* **2022**, *654*, 120557.
[178] E. Li, Z. Chen, C. Duan, B. Yuan, S. Yan, X. Luo, F. Pan, Z. Jiang, *Sep. Purif. Technol.* **2022**, *289*, 120714.
[179] E. Kamio, M. Tanaka, Y. Shirono, Y. Keun, F. Moghadam, T. Yoshioka, K. Nakagawa, H. Matsuyama, *Ind. Eng. Chem. Res.* **2020**, *59*, 2083.
[180] M. Zhang, L. Chen, K. Wang, R. Lin, Z. Xiao, R. Semiat, X. He, *ACS Appl. Polym. Mater* **2024**, *6*.
[181] S. He, E. Kamio, A. Matsuoka, K. Nakagawa, T. Yoshioka, H. Matsuyama, *J. Membr. Sci.* **2024**, *695*, 122482.
[182] S. Janakiram, X. Yu, L. Ansaloni, Z. Dai, L. Deng, *ACS Appl. Mater. Interfaces* **2019**, *11*, 33302.
[183] Z. Dai, J. Deng, Q. Yu, R. M. Helberg, S. Janakiram, L. Ansaloni, L. Deng, *ACS Appl. Mater. Interfaces* **2019**, *11*, 10874.
[184] R. Borgohain, B. Mandal, *ACS Appl. Mater. Interfaces* **2019**, *11*, 42616.
[185] N. Li, Z. Wang, J. Wang, *J. Membr. Sci.* **2022**, *642*, 119946.
[186] P. Jiamjirangkul, T. Inprasit, V. Intasanta, A. Pangon, *Chem. Eng. Sci.* **2020**, *221*, 115650.
[187] Z. Zhang, S. Rao, Y. Han, R. Pang, W. W. Ho, *J. Membr. Sci.* **2021**, *638*, 119696.
[188] T.-Y. Chen, X. Deng, L.-C. Lin, W. W. Ho, *J. Membr. Sci.* **2023**, *671*, 121309.

[189] G. Moad, E. Rizzardo, S. H. Thang, *Polymer* **2008**, *49*, 1079.
[190] J. Chiefari, Y. K. Chong, F. Ercole, J. Krstina, J. Jeffery, T. P. T. Le, R. T. A. Mayadunne, G. F. Meijs, C. L. Moad, G. Moad, *Macromolecules* **1998**, *31*, 5559.
[191] D. J. Keddie, G. Moad, E. Rizzardo, S. H. Thang, *Macromolecules* **2012**, *45*, 5321.
[192] G. Moad, E. Rizzardo, S. H. Thang, *Aust. J. Chem.* **2005**, *58*, 379.
[193] G. Moad, E. Rizzardo, S. H. Thang, *Aust. J. Chem.* **2006**, *59*, 669.
[194] G. Moad, E. Rizzardo, S. H. Thang, *Aust. J. Chem.* **2009**, *62*, 1402.
[195] G. Moad, E. Rizzardo, S. H. Thang, *Aust. J. Chem.* **2012**, *65*, 985.
[196] G. Moad, E. Rizzardo, S. H. Thang, *Chem. –Asian J.* **2013**, *8*, 1634.
[197] Y. K. Chong, T. P. T. Le, G. Moad, E. Rizzardo, S. H. Thang, *Macromolecules* **1999**, *32*, 2071.
[198] J. Rosselgong, E. G. L. Williams, T. P. Le, F. Grusche, T. M. Hinton, M. Tizard, P. Gunatillake, S. H. Thang, *Macromolecules* **2013**, *46*, 9181.
[199] X. Zhang, J. Wang, S. Zhou, S. Sun, X. Wang, S. Guo, F. Zhao, *J. Fluoresc.* **2022**, *32*, 435.
[200] X. Guo, X. Ji, X. Li, J. Du, L. Sun, A. Feng, J. Yuan, S. H. Thang, *Macromol. Rapid Commun.* **2021**, *42*, 2100019.
[201] J. Arredondo, N. M. Woodcock, O. Garcia-Valdez, P. G. Jessop, P. Champagne, M. F. Cunningham, *Langmuir* **2020**, *36*, 13989.
[202] X. Zhao, J. Zhang, Y. Zhao, *Polym. J.* **2020**, *52*, 153.
[203] X. Guo, W. Shi, H. Yin, J. Pan, Z. Wang, A. Feng, S. H. Thang, *Macromol. Rapid Commun.* **2021**, *42*, 2000765.
[204] X. Guo, T. Zhang, Y. Wu, W. Shi, B. Choi, A. Feng, S. H. Thang, *Polym. Chem.* **2020**, *11*, 6794.
[205] F. Yin, B. Lonetti, J.-D. Marty, N. Lauth-de Viguerie, *Colloids Surf. A: Physicochem. Eng. Asp.* **2023**, *674*, 131930.
[206] K. Wang, L. An, G. Lu, J. Zhang, Z. Wang, M. Si, G. Liu, Y. Zeng, *Polymer* **2023**, *280*, 126039.
[207] K. Wang, J. Zhang, M. Si, Z. Wang, L. An, G. Liu, Y. Zeng, *Macromolecules* **2023**, *56*, 9127.
[208] N. Haridharan, G.-J. Lee, S. Anandan, A. Sorrentino, Y.-H. Chuang, C.-H. Liu, J. J. Wu, *Environ. Technol.* **2022**, *43*, 3945.
[209] T. Tiainen, J. K. Mannisto, H. Tenhu, S. Hietala, *Langmuir* **2021**, *38*, 5197.
[210] N. Politakos, L. Serrano Cantador, J. A. Cecilia, I. Barbarin, R. Tomovska, *Appl. Sci.* **2021**, *11*, 11154.
[211] P. Nellepalli, L. C. Tome, K. Vijayakrishna, I. M. Marrucho, *Ind. Eng. Chem. Res.* **2019**, *58*, 2017.
[212] M. R. Moradi, H. Ramezanipour Penchah, A. Ghaemi, *Can. J. Chem. Eng.* **2023**, *101*, 5621.
[213] G. O. Aksu, I. Erucar, Z. P. Haslak, S. Keskin, *Chem. Eng. J.* **2022**, *427*, 131574.
[214] H. Zhang, S. Liu, L. Wang, H. Fang, X. Yue, Z. Wang, S. Wei, S. Liu, X. Lu, *Sep. Purif. Technol.* **2024**, *333*, 125937.
[215] T. Yan, M. Tong, D. Liu, Q. Yang, C. Zhong, *J. Mater. Chem. A* **2023**, *11*, 14911.
[216] X. Deng, C. Zou, Y. Han, L.-C. Lin, W. W. Ho, *J. Phys. Chem. C* **2020**, *124*, 25322.
[217] L. Meng, T. Kai, S.-i. Nakao, K. Yogo, *Int. J. Greenhouse Gas Control* **2023**, *123*, 103830.

Made Ganesh Darmayanti completed her Masters in Chemistry at Bandung Institute of Technology, Indonesia, in 2013. Since 2014 until present, she is a lecturer in the Faculty of Mathematics and Natural Sciences, University of Mataram, Indonesia. Currently, she is pursuing her Ph.D. degree in Chemistry at Monash University, Australia, under the supervision of Prof. San Thang and Prof. Kellie Tuck. Her research interests include exploring natural polymers through the RAFT polymerization approach and the application of polymeric materials and membrane for CO_2 capture.

Kellie L. Tuck is a professor at the School of Chemistry, Monash University. She obtained her Ph.D. from the University of Adelaide and subsequently held postdoctoral research positions at the University of South Australia, Australia, and the University of Cambridge, UK, before returning to Australia. Her research primarily centers on synthesising functional molecules for diverse applications, spanning supramolecular chemistry, medicinal chemistry, and sustainable surfactant development. She is engaged in a number of interdisciplinary research programs that combine organic chemistry with analytical chemistry, chemical engineering, and/or biology.

San H. Thang completed his Ph.D. in chemistry at Griffith University, Brisbane Australia in 1987. After a research career at the Commonwealth Scientific Industrial Research Organization (CSIRO) in Australia (1986–2014), he is currently a professor of Chemistry at Monash University. He is responsible for several key inventions in the area of controlled/living radical polymerization; significantly, he is a coinventor of the Reversible Addition-Fragmentation Chain Transfer (RAFT) process. Presently, he leads a research group with a primary focus on polymer synthesis by the RAFT process and developing RAFT polymers for industrial and biomedical applications.